TAMPEREEN TEKNILLINEN YLIOPISTO
TAMPERE UNIVERSITY OF TECHNOLOGY

SAEED KARIMI

# THREE DIMENSIONAL NUMERICAL SIMULATION, DESIGN AND STRUCTURAL OPTIMIZATION OF PNEUMATICALLY ACTUATED CELL STRETCHING DEVICE

Master of Science Thesis

Examiner: Professor Pasi Kallio
Supervisor: MSc. Joose Kreutzer
Examiner and topic approved by the Council of the Faculty of Engineering Sciences on 04.11.2015.

# ABSTRACT

TAMPERE UNIVERSITY OF TECHNOLOGY
Master's Degree Programme in Machine Automation
**KARIMI, SAEED**: Three Dimensional Numerical Simulation, Design and Structural Optimization of Pneumatically Actuated Cell Stretching Device
Master of Science Thesis, 64 pages
July 2016
Major: Micro-Machines
Examiner: Professor Pasi Kallio
Supervisor: M.Sc, Joose Kreutzer
Keywords: Cell Culturing, Cell's Mechanical Stimulation, Stress, Strain, Hyperelasticity, PolyDiMethylSiloxane (PDMS), Finite Element Method (FEM), Optimization

Utilizing biomimetic mechanical forces for differentiation of stem cells toward osteogenic, cardiomyocytes and other cell types is a technique that has been applied increasingly in recent years. Different types of apparatuses and devices are being designed and fabricated in order to accurately direct these mechanical forces onto stem cells in both 2D and 3D configurations.

In this thesis, a novel and easy-to-fabricate structure is designed to provide mechanical stimulation of cells in a cell culture environment. This is facilitated by means of pneumatic actuation. The pneumatic actuation of the hyperelastic PolyDiMethylSiloxane (PDMS) material directs a tensile strain on cell population in the environment. The structure has been previously designed at Micro- and Nanosystems research group to provide equiaxial strain. In this study, steps are taken to modify the structure to provide not only the equiaxial strain, but also uniaxial strain for stimulation of stem cells *in vitro*. As the primary objective of this study, the modified structure makes two aforementioned types of mechanical strain achievable.

In this study, computational model of the device is developed based on Neo-Hookean hyperelastic material model using COMSOL Multiphysics 5.1 software. Finite element based model of the structure is implemented and numerical simulations are performed to analyze stress and strain under applied vacuum. The structure is then optimized based on various geometric parameters to improve the performance of the device according to defined requirements and objective functions. The optimized structure is then further analyzed to completely identify the performance characteristics of the device.

Two different geometries are proposed for the device structure. The designed structures are demonstrated to provide relatively good performance based on requirements. The structures provide rather high strain magnitude in case of equiaxial strain. In case of uniaxial strain, they provide a relatively high average value for the first principal strain and a low average value for the second principal strain. The structures also exhibit an almost uniform uniaxial strain field. The results indicate an acceptable performance of the devices in both cases.

# PREFACE

I would like to express my gratitude to my examiner, Prof. Pasi Kallio who has always been and will be my role model that I have always admired. I should thank him for providing me such an excellent research environment in Micro- and Nanosystems research group of Tampere University of Technology. I should also appreciate his full support during my academic career and his sublime personality.

I should also thank my supervisor, doctoral researcher Joose Kreutzer for his instructions and guidance during the fulfillment of this project.

I would like to express my sincere appreciation to Prof. Reijo Kouhia from Mechanical Engineering Dept. of TUT.

I would like to thank all my colleagues at Micro- and Nanosystems research group, especially Jari Väliaho and Antti Mäki.

At last I would like to thank my family and loved ones.

# TABLE OF CONTENTS

# LIST OF SYMBOLS

| | |
|---|---|
| $\mathbf{A}$ | Area |
| $\boldsymbol{b}$ | Arc length of the rigid parts in circular structure |
| $\boldsymbol{C_{ij}}$ | Material constant in Neo-Hookean hyperelastic material law |
| $\boldsymbol{D_k}$ | Material constant in Neo-Hookean hyperelastic material law |
| $\boldsymbol{e}$ | Change in volume per unit volume |
| $\boldsymbol{E}$ | Modulus of elasticity or Young's modulus |
| $\boldsymbol{g}$ | Gap size between the rings in PDMS structure |
| $\boldsymbol{G}$ | Shear modulus, or modulus of rigidity |
| $\boldsymbol{h}$ | Height of the rigid parts |
| $\boldsymbol{I}$ | Invariant of stress |
| $\boldsymbol{J}$ | Invariant of strain |
| $\boldsymbol{k}$ | Bulk modulus |
| $\boldsymbol{L}$ | Original length of a line segment |
| $\boldsymbol{p}$ | Uniform pressure |
| $\mathbf{Q}, \mathbf{Q}'$ | Points on a body |
| $\boldsymbol{s}$ | Maximum distance of the rigid parts and the PDMS in oval structure |
| $\boldsymbol{S}$ | Stress vector |
| $\boldsymbol{t}$ | Thickness of the inner cylindrical shell in PDMS structure |
| $\boldsymbol{u}$ | Displacement component in x direction |
| $\boldsymbol{v}$ | Displacement component in y direction |
| $\boldsymbol{V}$ | Volume |

| | |
|---|---|
| $\boldsymbol{w}$ | Displacement component in z direction |
| $\boldsymbol{W}$ | Strain energy density |
| $\boldsymbol{W_d}$ | Deviatoric strain energy density |
| $\boldsymbol{W_v}$ | Volumetric strain energy density |
| $[\boldsymbol{\alpha}]$ | Matrix of direction cosines |
| $\boldsymbol{\gamma_{ij}}$ | Shear strain associated with i and j orthogonal directions |
| $\Delta\boldsymbol{A}$ | Area on a body surface |
| $\Delta\boldsymbol{L}$ | Change in length due to deformation |
| $\Delta\boldsymbol{P}$ | Force acting on a body surface |
| $\boldsymbol{\Delta V}$ | Change in volume |
| $\boldsymbol{\varepsilon}$ | Normal strain |
| $\boldsymbol{\varepsilon_a}$ | Axial strain |
| $\boldsymbol{\varepsilon_{ij}}$ | Tensorial shear strain |
| $\boldsymbol{\varepsilon_t}$ | Transverse strain |
| $\boldsymbol{\Theta}$ | Polar angle of the arc length of the rigid parts in oval structure |
| $\boldsymbol{\lambda}$ | First Lame´ constant |
| $\boldsymbol{\Lambda}$ | Stretch ratio |
| $\boldsymbol{\mu}$ | Second Lame´ constant |
| $\boldsymbol{\nu}$ | Poisson’s ratio |
| $\boldsymbol{\sigma}$ | Normal stress |
| $\boldsymbol{\sigma_a}$ | Uniaxial stress |
| $\boldsymbol{\sigma_{ij}}$ | Stress acting on the I face in j direction |
| $\boldsymbol{\tau}$ | Shear Stress |

# LIST OF ABBREVIATIONS

| | |
|---|---|
| FE | Finite Element |
| FEA | Finite Element Analysis |
| FEM | Finite Element Method |
| OF | Objective Functions |
| PDMS | PolyDiMethylSiloxane |
| TUT | Tampere University of Technology |

# LIST OF FIGURES

# LIST OF TABLES

# 1. INTRODUCTION

This chapter provides an introduction to the role of mechanical stimulation on stem cell growth and differentiation. The effects of two different common types of mechanical stimulation, i.e. uniaxial stretching and equiaxial stretching, on cells are explained. State of the art in existing equiaxial cell stretching device designed by Micro- and Nanosystems research group is depicted and the motivation to implement this study is also described.

## 1.1. Role of Mechanical Stimulation on Stem Cell Growth and Differentiation

Applying biomimetic mechanical forces for differentiation of stem cells toward osteogenic, cardiomyocytes and other cell types is a technique that has been practiced increasingly in recent years. Different types of apparatuses and devices are being designed and fabricated in order to accurately direct these mechanical forces onto stem cells in both 2D and 3D configurations. Currently, tensile strains are the most studied and widely used types of mechanical forces among all types of mechanical forces. Researches are also dedicated to making use of more complex systems, providing such forces as torsion, shearing, and hemodynamic forces. The effects of compressive forces and tensile strain on mesenchymal stem cells, adipose derived stem cells, and embryonic stem cells are in the interest of researchers in tissue engineering [1][2].

One of the key concepts in functional tissue engineering is determination of force pattern exposure of tissues *in vivo* [2]. The type of these force patterns and magnitude of these forces have been extensively modeled. These models are used in the design of bioreactors, which are intended to promote the *in vitro* recreation of the physiological environment that a specific tissue experiences *in vivo* [3].

It has been proven that utilizing different types of mechanical loads regulates the self-renewal of stem cells and directs their differentiation. However, the actual intracellular mechanisms through which this stem cell differentiation occurs, still remains largely unknown [5].

As mentioned earlier, it has been demonstrated that microenvironment of the stem cells influences their differentiation and phenotypic expression [6]. It is an engineering issue to make sure that applied forces *in vitro* are transmitted to the cells just as they would be experienced *in vivo*. Thus, understanding of biological systems in conjunction with the engineering ability to accurately recreate proper physical signals is required.

## 1.2. Tensile Forces

Tensile forces are one of the two main types of forces (the other one is compressive forces) applied to assist and direct the differentiation of stem cells toward a specific cell type. The two common forms of tensile strain deployed to achieve this goal are equi-axial and uniaxial strains.

### 1.2.1. Equiaxial Strain

Equiaxial strain is defined as a circumferential deformation that is equal in magnitude along all axes. The most common method to achieve equiaxial strain is to induce the deformation in the central region of a circular circumferentially bound elastic structure. In this case, cells which are present in the deformed central region would be experiencing a radial tensile stress in all possible directions.

Most researches investigating impacts of mechanical stresses on stem cell populations to direct the differentiation phenomena rely on accurate implementation of the patterns and magnitude of mechanical forces that the differentiated tissue will eventually be exposed to, *in vivo*. Under specific circumstances, mechanical stimulation of cells, enables guiding cell orientation and structured matrix deposition. This is an imperative in highly structured tissues such as muscle, cartilage and bone and will also result in improvement of mechanical properties of final tissues, theoretically [1].

Equiaxial tensile strains are the most common form of forces applied in order to achieve myogenic lineage for cardiovascular system which is composed of smooth and cardiac muscle [7].

### 1.2.2. Uniaxial Strain

Uniaxial stretching implies that the stretch applied to the cells is directed only in one axis. Uniaxial stretching is also referred to as longitudinal stretching. A uniaxial or longitudinal strain is accomplished when deformation is directed along a single axis in the structure. To obtain uniaxial stretching more complex structure is required. It has been proven that the cells' alignment direction versus the axis in which stretching occurs influences the differentiation of the cells.

In extent of osteogenic differentiation, uniaxial stretching has been applied to both human adipose stem cells (hASCs) and human mesenchymal stem cells (hMSCs) and the results indicated evidence of upregulated differentiation in both cell types [8].

## 1.3. Equiaxial Cell-Stretching Device

Mechanical stimulation of cells usually involves cell culture systems with controlled delivery of mechanical input such as hydrostatic pressure, fluid shear stress, or substrate strain [9]. PolyDiMethylSiloxane (PDMS) providing beneficial properties, such as: hyperelascticity, high transparency, gas permeability and non-toxicity, so that most mechanical cell stimulation devices are fabricated with PDMS. Furthermore, cell stimulation structures which utilize membrane deflection under pressure are commonly used in cell culturing due to ultra large deflections of PDMS and simplicity of the fabrication.

Micro- and Nanosystems research group has designed a novel system for studying cellular mechanobiology. The device is used to apply an equiaxial strain field to cells cultured on a PDMS base membrane. Cells under cultivation are stretched due to an existing equiaxial strain on the membrane of the device. This equiaxial strain field occurs as a result of deformation of the cylindrical shell under applied vacuum pressure.

This device has been designed and optimized in geometry to provide equiaxial in plane strain as high as possible along with out of plane displacement as low as possible. Figure 1.1 indicates the device assembly.

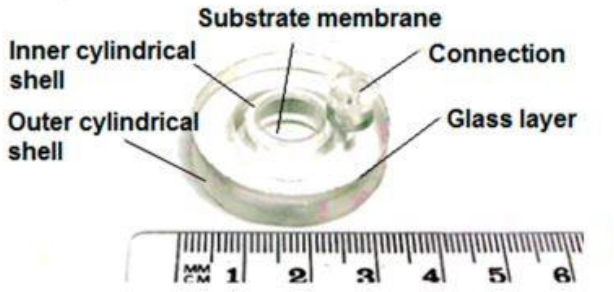


**Figure 1. 1.** Assembly of the novel cell stimulation device developed by Micro-Nanosystems research group at TUT [10]

The device consists of a PDMS cultivation membrane, an inner cylindrical shell, an outer cylindrical shell and a rigid glass layer. Inner and outer cylindrical shells are also made of PDMS. Vacuum pressure is applied to the device through a connection on top of the glass layer in the area between the inner and outer cylindrical shells.

Mechanical stimulation of the cells by equibiaxially expanding the membrane under vacuum pressure has been investigated previously in Micro-Nanosystems research group. In previous works [10][11][17], the structure has been studied to direct equiaxial strain for cell stimulation purposes and the structural geometry of the membrane has been optimized. Figure 1.2 presents the schematic view of the structure while deformed under applied vacuum pressure.

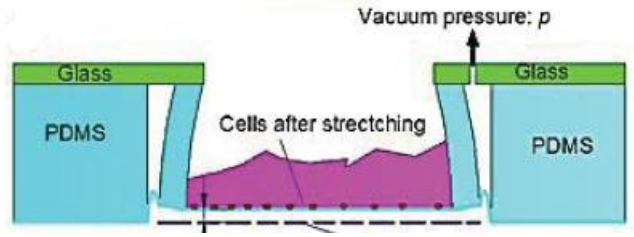


**Figure 1. 2.** Side view of the schematic diagram of the structure providing equiaxial strain after deflection [10]

## 1.4. Objectives and Motivations of the Study

The aforementioned structure is designed to direct an equiaxial strain to cells. In order to achieve a unidirectional strain by applying vacuum pressure, the structure is needed to be modified. Modifying and redesigning the structure in a manner to attain both equi-

axial and uniaxial strains with a single device is the primary objective of this thesis. The idea behind this study is to design a new housing and optimize this newly designed pneumatically actuated cell stretching device in order to obtain uniaxial strain in addition to equiaxial strain.

The research question that has been tried to reply in this thesis is: how is possible to achieve both types of equiaxial and uniaxial mechanical stimulation with only one single device which is also transparent, easy to fabricate and allows imaging of cells while experiencing mechanical stretching to study the effects of stimulation on cells at time of stimulation.

The incentive of this study is to use the same base structure which includes two inner and outer PDMS rings and a base membrane for both modes of operation, i.e. equiaxial and uniaxial. For this purpose, the main task is to discover an optimized cover plate with specific rigid features to restrict the displacement in one direction and maintain the perpendicular strain. Then by changing the cover plate and using a blank plate without rigid features (Figure 1.3), the same base structure could provide equiaxial strain.

To meet the requirements and make the device operational in two different modes of operation, different concepts and features for the cover plate needs to be designed based on the theory of strain-displacement relationship. However, optimized geometrical features of the cover plate structure are demanded.

In order to optimize the structure, studying the function of the designed cover plates and their effects on the produced strain field is essential. To achieve this objective, numerical simulation tools are employed to optimize the cover plate so that the strain field on the membrane is as unidirectional and uniform as possible.

The design concepts follow the presumption that is mentioned in the following sections. External features of cover plate are designed to restrict the deformation of the base structure in one dimension, and liberate the displacement in the in plane perpendicular dimension. This results in a uniaxial strain on the membrane which is directed to cells under cultivation. Figure 1.3 illustrates one of the design concepts for uniaxial stretching and it also demonstrates that the same PDMS structure is capable of providing equiaxial strain by changing the cover plate.

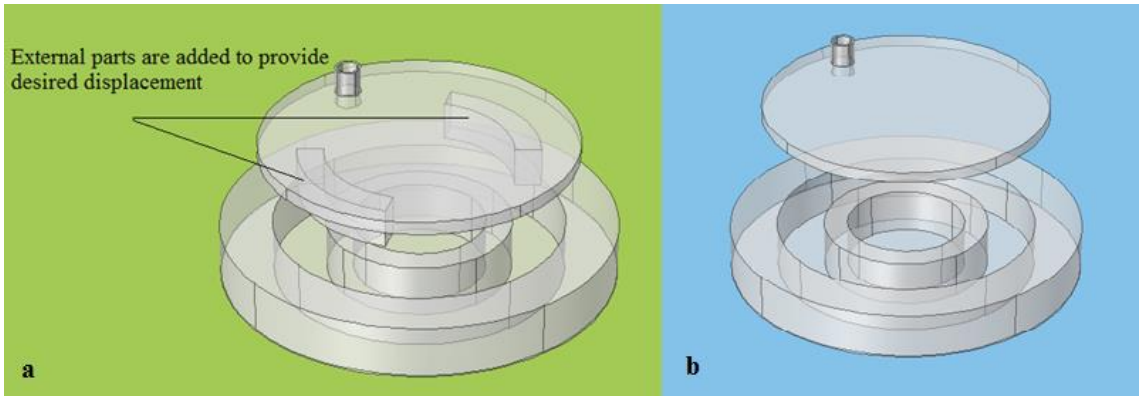


**Figure 1. 3.** (a) Design concept to allow obtaining uniaxial strain, (b) Different cover plate, results in eqiuaxial stretching with the same structure

## 1.5. Thesis Outline

This thesis is structured as follows. Chapter 2 gives a general introduction of mechanics of deformable bodies, theory of hyperelasticity and properties of PDMS. In Chapter 3, research methods used in this study are provided. The conceptual design of the structure and the implementation of the finite element based model of the structure in COMSOL Multiphysics 5.1 software are discussed. This chapter also includes definitions of objective functions required for an optimal case. In the following chapter, Chapter 4, the results of the numerical simulations are provided and discussed. Chapter 5 is meant to serve as a conclusion of this study, giving brief performance characteristics of the designed structures. Additionally, Chapter 5 contains a plan for future work.

# 2. THEORETICAL BACKGROUND

This chapter is devoted to express the theoretical framework of this study. Theories in the mechanics of deformable bodies and the theory of hyperelasticity are discussed and mathematical expressions of the common terms in the mechanics of deformable bodies are explained. Furthermore, material properties of PolyDiMethylSiloxan (PDMS) are described.

## 2.1. Mechanics of Deformable Bodies

Mechanics of deformable bodies deal with distribution of forces inside bodies, and the deformations caused by these internal force distributions. These internal forces cause stresses in the body. Principles of mechanics of deformable bodies are developed to analyze these internal stresses, and resulting deformations.

### 2.1.1. Stress and Strain at a Point

Stress is described as intensity of force. In a general state of loading, the stress vector **S** acting on section **D** at point **Q** is defined as:

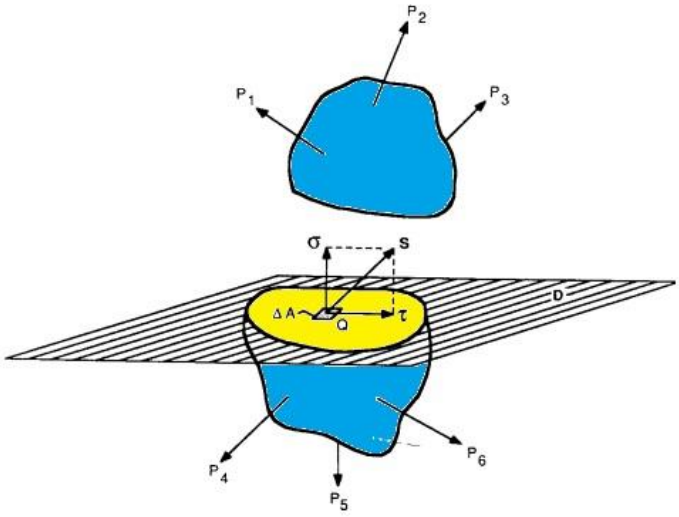


**Figure 2. 1.** Normal and shear stress [12]

$$S = \lim_{\Delta A \to 0} \frac{\Delta P}{\Delta A} \tag{1}$$

Where $\Delta P$ is the force acting on the area $\Delta A$. The stress vector **S**, denoted in Figure 2.1 can be divided into a normal and a tangential component to the section **D**. The normal component is referred to as normal stress and is denoted by $\boldsymbol{\sigma}$. The tangential component is called shear stress and is denoted by $\boldsymbol{\tau}$. The shearing stress $\boldsymbol{\tau}$ can be further divided into two orthogonal components, thus yielding an orthogonal triad of stress components.

Considering different sections through the same point in a body under load, different stress vectors will be obtained. To be able to specify the state of stress at a point, stresses acting on three mutually orthogonal sections at that point are taken into account.

Consider an infinitesimally small cube at the point of interest (see Fig. 2.2); $\boldsymbol{\sigma_{ij}}$ denotes the stress acting on the $\boldsymbol{i}$ face in the $\boldsymbol{j}$ direction, where $\boldsymbol{i}$ and $\boldsymbol{j}$ can be any of $\boldsymbol{x, y}$ or $\boldsymbol{z}$. Therefore, the state of stress at a point is represented in matrix form as:

$$\left[\sigma_{ij}\right] = \begin{bmatrix} \sigma_{xx} & \sigma_{xy} & \sigma_{xz} \\ \sigma_{yx} & \sigma_{yy} & \sigma_{yz} \\ \sigma_{zx} & \sigma_{zy} & \sigma_{zz} \end{bmatrix} \tag{2}$$

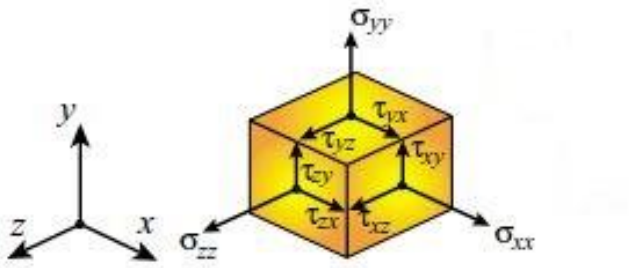


**Figure 2. 2.** General state of stress [12]

Matrix diagonal terms; $\boldsymbol{\sigma_{xx}}$, $\boldsymbol{\sigma_{yy}}$ and $\boldsymbol{\sigma_{zz}}$, represent the normal stress components in the coordinate system directions; $\boldsymbol{x, y}$ and $\boldsymbol{z}$, respectively. The off-diagonal terms of the matrix represent the shear stress components acting on the body. If the outward normal of the $\boldsymbol{i}$ face acts in the same direction as the positive $\boldsymbol{i}$ axis of the coordinate, the $\boldsymbol{i}$ face is considered positive and vice versa. The stress $\boldsymbol{\sigma ij}$**,** acting on the positive $\boldsymbol{i}$ face in the positive $\boldsymbol{j}$ direction or acting on the negative $\boldsymbol{i}$ face in the negative $\boldsymbol{j}$ direction, is considered to be positive, otherwise it is considered as negative. A positive normal stress is a tensile stress while a negative normal stress is called a compressive stress. In case of static equilibrium, it can be demonstrated that the cross-shearing stresses are equal, i.e. $\sigma_{xy} = \sigma_{yx}, \sigma_{xz} = \sigma_{zx}$ and $\sigma_{yz} = \sigma_{zy}$. Thus, the total number of stress components required to define the state of stress at a point in static equilibrium is reduced to six.

Movement of the points in a body relative to each other is defined as deformation and strain is describing the intensity of deformation. The normal strain at a point **Q** in the $x$ direction, $\varepsilon_{xx}$, is defined as:

$$\varepsilon_{xx} = \lim_{L \to 0} \frac{\Delta L}{L} \tag{3}$$

Where, L is the original length of a line segment centered at **Q** in the $x$ direction, and $\Delta L$ is the change in the length due to the deformation. A positive normal strain causes an increase in the length of the line segment and a decrease in length of the line segment is introduced by a negative normal strain. The shear strain associated with the orthogonal x and y directions, $\gamma_{xy}$, describes the change in the angle between infinitesimal line segments originally in the $x$ and $y$ directions before deformation. Shear strains which cause a reduction in the angle, are considered positive while negative shear strains result in an increase in angle. According to this definition, $\gamma_{xy} = \gamma_{yx}$, and no discontinuities occur at the point of interest. Figure 2.3 describes how shear strain is defined.

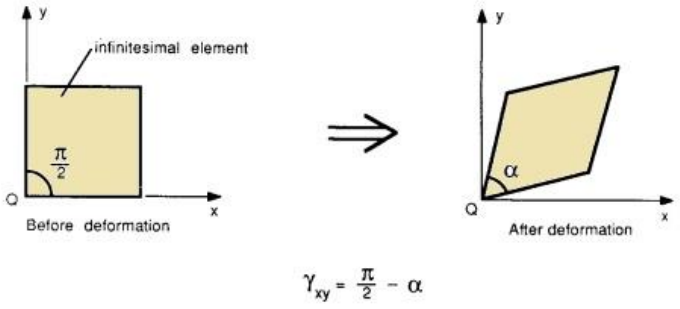


**Figure 2. 3.** Shear strain definition [12]

Tensorial shear strains $\varepsilon_{ij}$, defined to be half of the ordinary shear strains $\gamma_{ij}$. i.e. $\varepsilon_{ij} = \gamma_{ij}/2$ for $i \neq j$. Utilizing the tensorial shear strains, the state of strain at a point is represented in matrix form as:

$$[\varepsilon_{ij}] = \begin{bmatrix} \varepsilon_{xx} & \varepsilon_{xy} & \varepsilon_{xz} \\ \varepsilon_{yx} & \varepsilon_{yy} & \varepsilon_{yz} \\ \varepsilon_{zx} & \varepsilon_{zy} & \varepsilon_{zz} \end{bmatrix} \tag{4}$$

The diagonal terms are the normal strain components and the off-diagonal terms are the tensorial shear strain components. The strain is a dimensionless quantity.

## 2.1.2. Strain-Displacement Relations

Strains are related to derivatives of displacements mathematically. Considering a point **Q** in a body displaces to point **Q´**, when it undergoes a deformation by application of load. Assuming $u, v$ and $w$ to be displacement components of the primary point in the

$x, y$ and $z$ directions, respectively, the strain components are obtained as below according to previously given definition of normal and shear strains.

$$\varepsilon_{xx} = \sqrt{1 + 2\frac{\partial u}{\partial x} + (\frac{\partial u}{\partial x})^2 + (\frac{\partial v}{\partial x})^2 + (\frac{\partial w}{\partial x})^2} - 1$$

$$\varepsilon_{yy} = \sqrt{1 + 2\frac{\partial v}{\partial y} + (\frac{\partial u}{\partial y})^2 + (\frac{\partial v}{\partial y})^2 + (\frac{\partial w}{\partial y})^2} - 1$$

$$\varepsilon_{zz} = \sqrt{1 + 2\frac{\partial w}{\partial z} + (\frac{\partial u}{\partial z})^2 + (\frac{\partial v}{\partial z})^2 + (\frac{\partial w}{\partial z})^2} - 1$$

$$\gamma_{xy} = \gamma_{yx} = \sin^{-1}\left[\frac{\frac{\partial u}{\partial y} + \frac{\partial v}{\partial x} + \frac{\partial u}{\partial x}\frac{\partial u}{\partial y} + \frac{\partial v}{\partial x}\frac{\partial v}{\partial y} + \frac{\partial w}{\partial x}\frac{\partial w}{\partial y}}{(1 + \varepsilon_{xx})(1 + \varepsilon_{yy})}\right] \tag{5}$$

$$\gamma_{xz} = \gamma_{zx} = \sin^{-1}\left[\frac{\frac{\partial w}{\partial x} + \frac{\partial u}{\partial z} + \frac{\partial w}{\partial z}\frac{\partial w}{\partial x} + \frac{\partial u}{\partial z}\frac{\partial u}{\partial x} + \frac{\partial v}{\partial z}\frac{\partial v}{\partial x}}{(1 + \varepsilon_{xx})(1 + \varepsilon_{zz})}\right]$$

$$\gamma_{yz} = \gamma_{zy} = \sin^{-1}\left[\frac{\frac{\partial v}{\partial z} + \frac{\partial w}{\partial y} + \frac{\partial v}{\partial y}\frac{\partial v}{\partial z} + \frac{\partial w}{\partial y}\frac{\partial w}{\partial z} + \frac{\partial u}{\partial y}\frac{\partial u}{\partial z}}{(1 + \varepsilon_{yy})(1 + \varepsilon_{zz})}\right]$$

The higher order terms in the equations above, can be neglected in case the displacements and strains are sufficiently small, and the equations reduce to:

$$\varepsilon_{xx} = \frac{\partial u}{\partial x}$$

$$\varepsilon_{yy} = \frac{\partial v}{\partial y}$$

$$\varepsilon_{zz} = \frac{\partial w}{\partial z}$$

$$\gamma_{xy} = \gamma_{yx} = \frac{\partial v}{\partial x} + \frac{\partial u}{\partial y} \tag{6}$$

$$\gamma_{xz} = \gamma_{zx} = \frac{\partial w}{\partial x} + \frac{\partial u}{\partial z}$$

$$\gamma_{yz} = \gamma_{zy} = \frac{\partial w}{\partial y} + \frac{\partial v}{\partial z}$$

## 2.1.3. Linear Elastic Stress-Strain Relationships

Stresses and strains are generally not independent, but rather related to each other. The exact form of stress-strain relationships depends on the mechanical properties of the material; whether behaving as elastic, viscoelastic, hyperelastic or some other fashion.

Elastic response of a body determines that the body returns to its original shape upon removal of loads. If, in addition, the stress - strain relationship is linear, the member is said to be experiencing linear elastic response.

**Axial Loading**

In case of uniaxial loading, the stress-strain relationship is:

$$\sigma_a = \frac{P}{A} = E\varepsilon_a \tag{7}$$

Where $P$ is the applied axial force, $A$ is the cross-sectional area, $\varepsilon_a$ is the axial strain, and $E$ is a material constant named modulus of elasticity or Young's modulus. This equation is known as Hooke's law. The transverse strain, $\varepsilon_t$, is derived from:

$$\varepsilon_t = -\nu\varepsilon_a = -\frac{\nu\sigma_a}{E} \tag{8}$$

Where $\nu$ is a material constant known as Poisson's ratio. Its value is always between 0 and $\frac{1}{2}$ for linear elastic, isotropic[1] response.

**Multiaxial State of Stress**

In the general case of three-dimensional state of stress, the stress-strain relationships are given by Equations 9.

$$\begin{aligned} \varepsilon_{xx} &= \frac{1}{E}\left[\sigma_{xx} - \nu\left(\sigma_{yy} + \sigma_{zz}\right)\right] & \gamma_{xy} &= \frac{\sigma_{xy}}{G} \\ \varepsilon_{yy} &= \frac{1}{E}\left[\sigma_{yy} - \nu(\sigma_{xx} + \sigma_{zz})\right] & \gamma_{yz} &= \frac{\sigma_{yz}}{G} \\ \varepsilon_{zz} &= \frac{1}{E}\left[\sigma_{zz} - \nu\left(\sigma_{xx} + \sigma_{yy}\right)\right] & \gamma_{zx} &= \frac{\sigma_{zx}}{G} \end{aligned} \tag{9}$$

**G** is a material constant named shear modulus, or modulus of rigidity. These equations are referred to as the generalized Hooke's law.

Inverting the above equations yields the stresses in terms of the strains, visible in Equations 10.

$$\begin{aligned} \sigma_{xx} &= \frac{E}{(1+\nu)(1-2\nu)}\left[(1-\nu)\varepsilon_{xx} + \nu\left(\varepsilon_{yy} + \varepsilon_{zz}\right)\right] & \sigma_{xy} &= G\gamma_{xy} \\ \sigma_{yy} &= \frac{E}{(1+\nu)(1-2\nu)}\left[(1-\nu)\varepsilon_{yy} + \nu(\varepsilon_{xx} + \varepsilon_{zz})\right] & \sigma_{yz} &= G\gamma_{yz} \\ \sigma_{zz} &= \frac{E}{(1+\nu)(1-2\nu)}\left[(1-\nu)\varepsilon_{zz} + \nu\left(\varepsilon_{xx} + \varepsilon_{yy}\right)\right] & \sigma_{zx} &= G\gamma_{zx} \end{aligned} \tag{10}$$

In the theory of elasticity, the material constants $G, E,$ and $\nu$ are not independent of each other, but they are related to each other by the Eq. 11.

$$G = E/2(1 + \nu) \tag{11}$$

In the theory of elasticity, change in volume per unit volume is presented by the dilatation $e$. In case of small strains, it is obtained by $e = \varepsilon_{xx} + \varepsilon_{yy} + \varepsilon_{zz}$. In case of pure hydrostatic stress; $\sigma_{xx} = \sigma_{yy} = \sigma_{zz} = -p$ and $\sigma_{xy} = \sigma_{yz} = \sigma_{zx} = 0$, where p is the uniform pressure acting on the body, the dilatation is linearly related to the pressure

[1] An isotropic material displays the same properties in all directions.

by $e = -p/k$, where $k$ is a material constant named bulk modulus. The bulk modulus is related to $E$ and $\nu$ by the Eq. 12.

$$k = E/3(1 - 2\nu) \tag{12}$$

Another elastic constant that arises in the theory of elasticity is, Lame´ constant, $\lambda$, which has no physical significance unlike the other constants; $E, \nu, G$, and $k$. In other words, there is no mechanical test to measure Lame´ constant directly. In order to completely describe a linear elastic isotropic behavior, only two material constants are required. Thus, the constants $E, \nu, G, k,$ and $\lambda$ can be interrelated.

### 2.1.4. Plane Stress and Strain

In case an orientation can be found such that the stress at a point in one of the three coordinates is zero; that is a two dimensional state of stress or plane stress. If the zero direction of the stress assumed to be the **z** direction, then:

$$\sigma_{zz} = \sigma_{xz} = \sigma_{yz} = 0 \tag{13}$$

And Equations 9 are reduced to:

$$\begin{aligned}
\varepsilon_{xx} &= \frac{1}{E}\left(\sigma_{xx} - \nu\sigma_{yy}\right) \\
\varepsilon_{yy} &= \frac{1}{E}\left(\sigma_{yy} - \nu\sigma_{xx}\right) \\
\varepsilon_{zz} &= \frac{-\nu}{E}\left(\sigma_{xx} + \nu\sigma_{yy}\right) \\
\gamma_{xy} &= \frac{\sigma_{xy}}{G} \\
\gamma_{xz} &= 0 \\
\gamma_{yz} &= 0
\end{aligned} \tag{14}$$

$\varepsilon_{zz}$, can also be written as:

$$\varepsilon_{zz} = \frac{-\nu}{1-\nu}\left(\varepsilon_{xx} + \varepsilon_{yy}\right) \tag{15}$$

Similarly, Equations 10 reduce to:

$$\sigma_{xx} = \frac{E}{1-\nu^2}(\varepsilon_{xx} + \nu\varepsilon_{yy})$$

$$\sigma_{yy} = \frac{E}{1-\nu^2}(\varepsilon_{yy} + \nu\varepsilon_{xx})$$

$$\sigma_{zz} = 0 \qquad (16)$$

$$\sigma_{xy} = G\gamma_{xy}$$

$$\sigma_{xz} = 0$$

$$\sigma_{yz} = 0$$

In case an orientation can be found such that the strain at a point in one of the three co-ordinates is zero; that is plane strain. If the zero direction of the strain assumed to be the ***z*** direction, then:

$$\varepsilon_{zz} = \gamma_{xz} = \gamma_{yz} = 0 \qquad (17)$$

And Equations 9 are reduced to:

$$\varepsilon_{xx} = \frac{1+\nu}{E}\left[(1-\nu)\sigma_{xx} - \nu\sigma_{yy}\right]$$

$$\varepsilon_{yy} = \frac{1+\nu}{E}\left[(1-\nu)\sigma_{yy} - \nu\sigma_{xx}\right]$$

$$\varepsilon_{zz} = 0 \qquad (18)$$

$$\gamma_{xy} = \frac{\sigma_{xy}}{G}$$

$$\gamma_{xz} = 0$$

$$\gamma_{yz} = 0$$

In addition, Equations 10 reduce to:

$$\sigma_{xx} = \frac{E}{(1+\nu)(1-2\nu)}\left[(1-\nu)\varepsilon_{xx} + \nu\varepsilon_{yy}\right]$$

$$\sigma_{xy} = G\gamma_{xy}$$

$$\sigma_{yy} = \frac{E}{(1+\nu)(1-2\nu)}\left[(1-\nu)\varepsilon_{yy} + \nu\varepsilon_{xx}\right] \tag{19}$$

$$\sigma_{xz} = 0$$

$$\sigma_{zz} = \frac{\nu E}{(1+\nu)(1-2\nu)}\left[\varepsilon_{xx} + \varepsilon_{yy}\right]$$

$$\sigma_{yz} = 0$$

$\sigma_{zz}$, can also be written as:

$$\sigma_{zz} = \nu\left(\sigma_{xx} + \sigma_{yy}\right) \tag{20}$$

## 2.1.5. Transformation of Stress and Strain

**General Transformation**

It is often necessary to obtain the state of stress or strain in a desired orientation while it has been primarily obtained in another orientation.

The matrix equation for transformation of stress from current ***Oxyz*** coordinate system to new ***Ox´y´z´*** coordinate system is given by:

$$\left[\sigma'\right] = [\alpha]^T[\sigma][\alpha] \tag{21}$$

$[\sigma]$ is the stress matrix for the original coordinate system and $\left[\sigma'\right]$ is the stress matrix for the new coordinate system.

$[\alpha]$ is the matrix of direction cosines and is given by[2]:

$$[\alpha] = \begin{bmatrix} \cos(x',x) & \cos(y',x) & \cos(z',x) \\ \cos(x',y) & \cos(y',y) & \cos(z',y) \\ \cos(x',z) & \cos(y',z) & \cos(z',z) \end{bmatrix} \tag{22}$$

$[\alpha]^T$ is the matrix transpose of $[\alpha]$.

[2] $\cos(i', j)$ represents the direction cosine between the original $j$ coordinate axis and new $i'$ coordinate axis

Similarly, for strain transformation:

$$[\varepsilon'] = [\alpha]^T[\varepsilon][\alpha] \tag{23}$$

**Transformation about a Fixed Axis**

In case of in plane orientation about the ***z*** axis by an angle $\boldsymbol{\theta}$ (i.e. $z' = z$), the equations are simplified to:

$$\begin{gathered}\cos(x', x) = \cos(y', y) = \cos\theta \\ \cos(y', x) = \cos(90° + \theta) \\ \cos(x', y) = \cos(90° - \theta) \\ \cos(z', x) = \cos(x', z) = \cos(z', y) = \cos(y', z) = 0 \\ \cos(z', z) = 1\end{gathered} \tag{24}$$

and:

$$\begin{gathered}\sigma'_{xx} = \tfrac{1}{2}(\sigma_{xx} + \sigma_{yy}) + \tfrac{1}{2}(\sigma_{xx} - \sigma_{yy})\cos 2\theta + \sigma_{xy}\sin 2\theta \\ \sigma'_{yy} = \tfrac{1}{2}(\sigma_{xx} + \sigma_{yy}) - \tfrac{1}{2}(\sigma_{xx} - \sigma_{yy})\cos 2\theta - \sigma_{xy}\sin 2\theta \\ \sigma'_{xy} = -\tfrac{1}{2}(\sigma_{xx} - \sigma_{yy})\sin 2\theta - \sigma_{xy}\cos 2\theta \\ \sigma'_{zz} = \sigma_{zz} \\ \sigma'_{xz} = \sigma_{xz} \\ \sigma'_{yz} = \sigma_{yz}\end{gathered} \tag{25}$$

and similarly:

$$\begin{gathered}\varepsilon_{xx}^{'} = \frac{1}{2}(\varepsilon_{xx} + \varepsilon_{yy}) + \frac{1}{2}(\varepsilon_{xx} - \varepsilon_{yy})\cos 2\theta + \varepsilon_{xy}\sin 2\theta \\ \varepsilon_{yy}^{'} = \frac{1}{2}(\varepsilon_{xx} + \varepsilon_{yy}) - \frac{1}{2}(\varepsilon_{xx} - \varepsilon_{yy})\cos 2\theta - \varepsilon_{xy}\sin 2\theta \\ \varepsilon_{xy}^{'} = -\frac{1}{2}(\varepsilon_{xx} - \varepsilon_{yy})\sin 2\theta - \varepsilon_{xy}\cos 2\theta \\ \varepsilon_{zz}^{'} = \varepsilon_{zz} \\ \varepsilon_{xz}^{'} = \varepsilon_{xz} \\ \varepsilon_{yz}^{'} = \varepsilon_{yz}\end{gathered} \tag{26}$$

## 2.1.6. Principal Stresses and Strains

For any state of stress at a point, a particular orientation can be defined such that the shear stresses vanish. In this particular orientation the stress matrix is given by:

$$[\sigma] = \begin{bmatrix}\sigma_1 & 0 & 0 \\ 0 & \sigma_2 & 0 \\ 0 & 0 & \sigma_3\end{bmatrix} \tag{27}$$

$\sigma_1, \sigma_2$, and $\sigma_3$ are called principal stresses. It is commonly assumed that the orientation has been chosen such that $\sigma_1$ is the largest algebraic stress and $\sigma_3$ is the smallest one.

The principal stresses are eigenvalues of the general symmetric stress tensor and represent the solutions to the cubic equation.

$$\sigma_n^3 - I_1\sigma_n^2 + I_2\sigma_n - I_3 = 0 \tag{28}$$

Where

$$\begin{gathered}I_1 = \sigma_{xx} + \sigma_{yy} + \sigma_{zz} \\ I_2 = \sigma_{xx}\sigma_{yy} + \sigma_{xx}\sigma_{zz} + \sigma_{yy}\sigma_{zz} - \sigma_{xy}^2 - \sigma_{yz}^2 - \sigma_{zx}^2 \\ I_3 = \sigma_{xx}\sigma_{yy}\sigma_{zz} - \sigma_{xx}\sigma_{yz}^2 - \sigma_{yy}\sigma_{zx}^2 - \sigma_{zz}\sigma_{xy}^2 + 2\sigma_{xy}\sigma_{xz}\sigma_{yz}\end{gathered} \tag{29}$$

$I_1, I_2,$ and $I_3$ are independent of the considered orientation and are known as the first, second, and third invariants of stress, respectively.

Similar to stresses, an orientation can be found such that the shear strains vanish, i.e. there exists an orthogonal set of axes 1, 2, and 3, with respect to which the tensor elements are all zero except for those in the diagonal. The principal strains; $\varepsilon_1, \varepsilon_2$, and $\varepsilon_3$, represent the solutions to the cubic equation

$$\varepsilon_n^3 - J_1\varepsilon_n^2 + J_2\varepsilon_n - J_3 = 0 \tag{30}$$

Where

$$\begin{aligned} J_1 &= \varepsilon_{xx} + \varepsilon_{yy} + \varepsilon_{zz} \\ J_2 &= \varepsilon_{xx}\varepsilon_{yy} + \varepsilon_{xx}\varepsilon_{zz} + \varepsilon_{yy}\varepsilon_{zz} - \varepsilon_{xy}^2 - \varepsilon_{yz}^2 - \varepsilon_{zx}^2 \\ J_3 &= \varepsilon_{xx}\varepsilon_{yy}\varepsilon_{zz} - \varepsilon_{xx}\varepsilon_{yz}^2 - \varepsilon_{yy}\varepsilon_{zx}^2 - \varepsilon_{zz}\varepsilon_{xy}^2 + 2\varepsilon_{xy}\varepsilon_{xz}\varepsilon_{yz} \end{aligned} \tag{31}$$

$J_1, J_2,$ and $J_3$ remain the same regardless of the orientation and respectively called the first, second, and third invariants of strain.

## 2.2. Theory of Hyperelasticity

In this section, the theory of hyperelasticity and laws for modelling hyperelastic materials are described. The Hyperelastic material model is a type of constitutive models for ideally elastic material. The stress-strain relationship of a hyperelastic material is derived from the strain energy density function.

### 2.2.1. Hyperelastic Materials

A hyperelastic material is still an elastic material which simply means that it returns to its original shape upon removal of forces. In addition to that, a hyperelastic material is obeying Cauchy-elastic materials definitions; meaning that the stress is determined by the current state of deformation, independent of the path or history of deformation. What makes hyperelastic materials different from linear elastic materials is that the stress-strain relationship is not a constant factor and it derives from the strain energy density function.

Elastomers are often modeled as hyperelastic. Elastomers typically provide large strains at small loads, i.e. very low modulus of elasticity and the material is nearly incompressible, i.e. the Poisson's ratio is very close to 0.5.

In hyperelastic materials, stress-strain curves during loading and unloading are not the same. Figure 2.4 compares the stress-strain curve in hyperelastic and linear elastic materials. As indicated, in hyperelastic materials the relation between stress and strain is nonlinear (Figure 2.4.a). However, in linear elastic materials the stress-strain relation (Figure 2.4.b) is linear. Hyperelastic materials provide larger strains compared to linear elastic materials under loading.

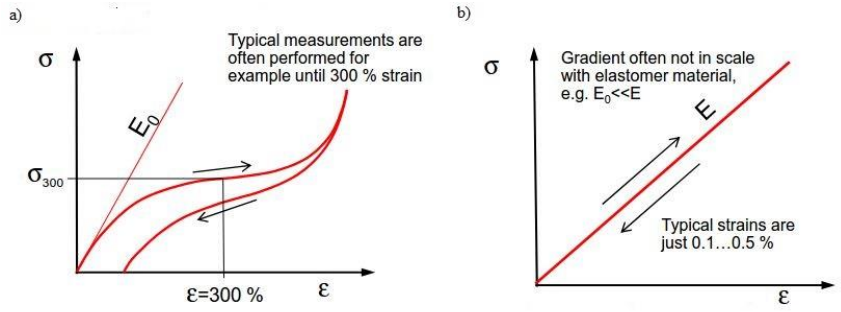


**Figure 2. 4.** Stress-Strain curve during loading and unloading; a. Hyperelastic material, b. Linear Elastic material [21]

## 2.2.2. Material Laws for Hyperelastic Materials

The nominal or engineering strain is defined as the change in length divided by the original length:

$$\varepsilon = \frac{\Delta L}{L} \tag{32}$$

Another fundamental quantity used to describe material deformation is the stretch ratio, Λ. It is defined as the current length divided by the original length.

$$\Lambda = \frac{l}{l_0} = \frac{l - l_0 + l_0}{l_0} = \varepsilon + 1 \tag{33}$$

Along to the three principal strains, we obtain three principal stretch ratios $\lambda_1, \lambda_2, \lambda_3$. The three stretch invariants which are:

$$\begin{aligned} I_1 &= \Lambda_1^2 + \Lambda_2^2 + \Lambda_3^2 \\ I_2 &= \Lambda_1^2\Lambda_2^2 + \Lambda_2^2\Lambda_3^2 + \Lambda_1^2\Lambda_3^2 \\ I_3 &= \Lambda_1^2\Lambda_2^2\Lambda_3^2 = 1 + (\frac{\Delta V}{V})^2 = J^2 \end{aligned} \tag{34}$$

Where J is the total volumetric ratio and its value is 1 for incompressible materials.

Compared to linear elastic materials where the stress is a linear function of strain, the description of the strain energy density, **W** is more complicated in hyperelastic materials.

As indicated in Figure 2.4.b, a straight line is obtained as the stress-strain characteristic curve when loading and unloading a linear elastic material. In this case the strain energy density, **W** is equal to half of the value of the double dot product of the stress tensor, **S** and the strain tensor, **E**:

$$W = \frac{1}{2}\, S \cdot\cdot E \tag{35}$$

In hyperelastic materials, generally the strain energy density is function of stretch invariants, $W = f(I_1, I_2, I_3)$, or principal stretch ratios, $W = f(\lambda_1, \lambda_2, \lambda_3)$.

Due to material incompressibility, the strain energy density function is split into distinct deviatoric $W_d$ and volumetric $W_V$ terms. Consequently, the volumetric term is only the function of the volume ratio J.

$$W = W_d(\bar{I}_1, \bar{I}_2) + W_V(J) \tag{36}$$

Or

$$W = W_d\left(\bar{\lambda}_1, \bar{\lambda}_2, \bar{\lambda}_3\right) + W_V(J) \tag{37}$$

In the equation, $W_d$ is the strain energy changing the shape, and $W_V$ is the strain energy to change the volume.

Phenomenological models of the strain energy function obtained for hyperelastic materials, is in the form of:

$$W = \sum_{i+j=1}^{N} C_{ij}(I_1 - 3)^i (I_2 - 3)^j + \sum_{k=1}^{N} \frac{1}{D_k}(J-1)^{2k} \tag{38}$$

$C_{ij}$ and $D_k$ are the material constants which are determined through experiment. This means, the strain energy function is a polynomial function and its order depends on N.

Variety of hyperelastic material laws have been developed to be used in modeling hyperelasticity. Some of those are; Neo-Hookean, Mooney-Rivlin, Ogden and Arruda-Boyce model.

**Neo-Hookean Model**

The Neo-Hookean model is the simplest approach to model hyperelastic materials. Equation 39 describes the Neo-Hookean hyperelastic material law.

$$W = C_{10}(\bar{I}_1 - 3) + \frac{1}{D_1}(J_e - 1)^2 \tag{39}$$

Equation 40 presents the Money-Rivlin hyperelastic material model.

**Mooney-Rivlin model:**

$$W = C_{10}(\bar{I}_1 - 3) + C_{01}(\bar{I}_2 - 3) + \frac{1}{D_1}(J_e - 1)^2 \tag{40}$$

Figure 2.5 describes how linear elastic, NeoHookean, and Mooney-Rivlin material laws express the stress-strain relationship for an incompressible material.

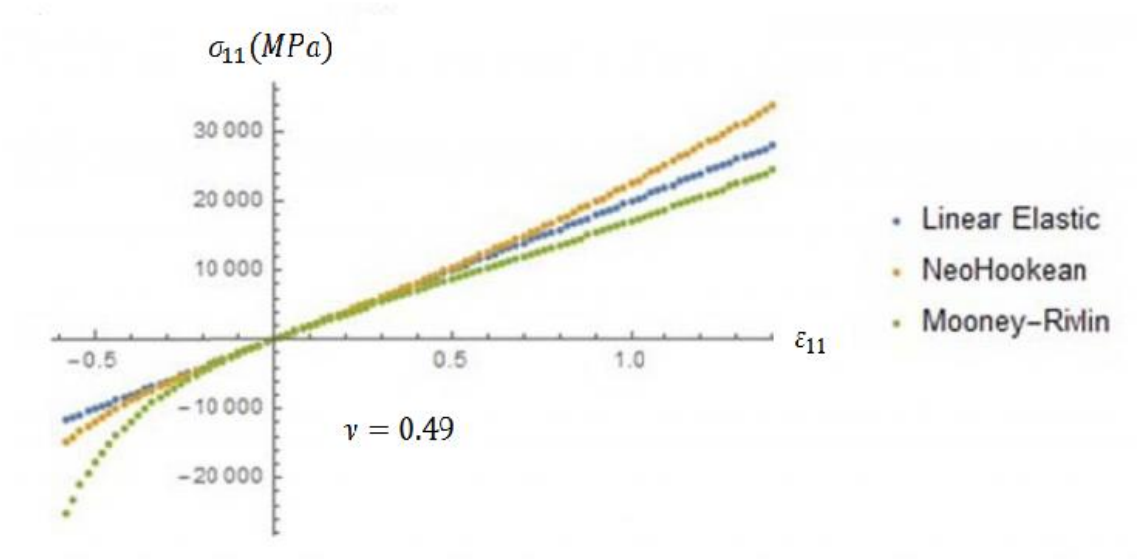


**Figure 2. 5.** Stress-Strain curve for Linear Elastic, Neo-Hookean, and Mooney-Rivlin material laws [22]

It can be realized that for small strains (less than 0.1) the three material models yield a similar result. However, as the strain increases, there are difference in yielded results.

## 2.3. PolyDiMethylSiloxane (PDMS)

PolyDiMethylSiloxane (PDMS) or Dimethicone is a polymer widely used for manufacturing microfluidic devices.

PDMS is a mineral-organic polymer (a structure containing carbon and silicon) belonging to siloxane (silicon, oxygen and alkane) family. To manufacture microfluidic devices, elastomer (in liquid state) mixed with a cross-linking agent is poured into a microstructured mold and heated to obtain a replica of the mold.

The empirical formula of PDMS is $(C_2H_6OSi)_n$ and fragmented formula is $CH_3[Si(CH_3)_2O]_nSi(CH_3)_3$, where n is the number of repetitions of the monomer. Figure 2.6 indicates the empirical formula of PDMS.

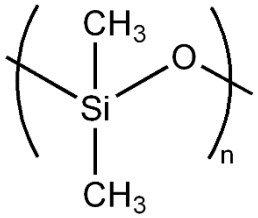


**Figure 2. 6.** Empirical formula of PDMS

### 2.3.1. General Properties of PDMS

Depending on the size of the string of monomer, the non-cross-linked PDMS may be almost liquid (low n) or semi-solid (high n). The siloxane bonds allow a flexible polymer chain with a high level of viscoelasticity to be obtained.

The ease of fabrication, biocompatibility, elastomeric property, transparency and low cost are the main attractions of PDMS to be utilized in rapid prototyping while PDMS is disfavored because of its hydrophobicity.

After cross-linking, PDMS becomes a hydrophobic elastomer, i.e. polar solvents such as water do not spread on the PDMS surface. The surface treatment is needed to control the wettability. The surface properties of PDMS are modified using different methods such as chemical coating [20, 23], thermal aging [24] and plasma oxidation [23].

Oxygen plasma treatment of PDMS introduces polar functional groups; mainly the silanol group (SiOH) to the surface which changes the surface properties of PDMS from being hydrophobic to hydrophilic. Hydrophilic surfaces improve wettability. However, the plasma treated hydrophilic surface of PDMS is unstable and low molecular weight (LMW) chains diffuse from the bulk of the PDMS and cover up the thermodynamically unstable surface [23]. Thus the characteristics of modified PDMS surfaces using plasma treatment are unstable and gradually changes during aging. LMW species are either uncross-linked linear PDMS chains or residual crosslinking agent. These LMW species can be volatilized and removed from the bulk through thermal aging [24]. A PDMS network without LMW species will retain its hydrophilicity for a much greater time.

The mechanical properties of PDMS enable the realization of pneumatic, electromagnetic, and thermal actuators. Table 2.1 represents the material properties of PDMS.

**Table 2. 1.** Material properties of PDMS, Sylgard 184 [14]

| Property | Characteristic | Consequence |
|---|---|---|
| **Optical** | Transparent; UV cutoff. 240 nm | Optical detection from 240 to 1100 nm |
| **Electrical** | Insulating; breakdown voltage, $2 \times 10^7 V/m$ | Allows embedded circuits; intentional breakdown to open connections |
| **Mechanical** | Elastomeric; tunable young modulus $E = [0.8 - 4]\ MPa$ | Conforms to surface; allows actuation by reversible deformation; facilitates release from molds |
| **Thermal** | Insulating; thermal conductivity, 0.2 $W(m \cdot K)$; coefficient of thermal expansion, 310 $\mu m/(m \cdot ℃)$ | Can be used to insulate heated solutions; does not allow dissipation of resistive heating from electrophoretic separation |
| **Interfacial** | Low surface free energy $\sim 20\ erg/cm^2$ | Replicas release easily from the mold; can be reversibly sealed with materials |
| **Permeability** | Impermeable to liquid water; permeable to gases and nonpolar organic solvents | Contains aqueous solutions in channels; allows gas transport through the bulk material; incompatible with many organic solvents |
| **Reactivity** | Inert; can be oxidized by exposure to a plasma; $Bu_4N^+F^-((TBA)F)$ | Unreactive toward most reagents; surface can be etched; can be modified to be hydrophilic and also reactive toward Silanes; etching with (TBA)F can alter the topography of surfaces |

### 2.3.2. Mechanical Properties

Cross-linked PDMS behaves as a rubbery solid, i.e. the polymer does not permanently deform under loading. Rather, the polymer is elastic and returns to its original shape when unloaded. The elastic property of PDMS is highly dependent on the amount of cross-linking agent integrated into the polymer. With little or without cross-linking

agent, the polymer remains as a viscous liquid, and as the concentration of cross-linking agent increases, the polymer becomes more solid. PDMS formulations span a wide range of mechanical properties from soft gels to stiff elastomers. Figure 2.7 illustrates the stress-strain curves[3] of four different mass ratios of the Sylgard 184:527; 5:1, 1:1, 1:5, and 1:10. According to [15], the samples were made by first preparing pure Sylgard 527 and 184, and then combining by the indicated mass ratio.

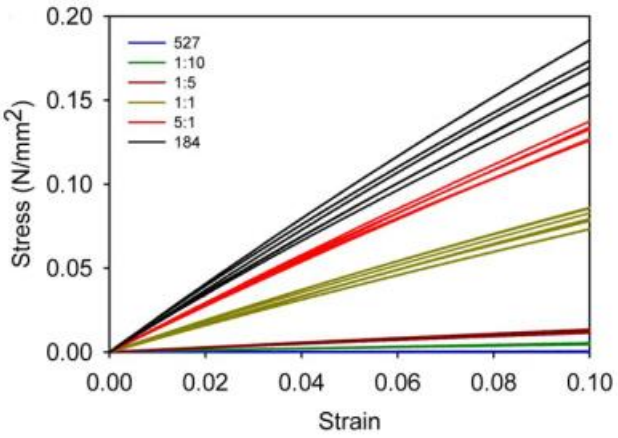


**Figure 2. 7.** Stress-Strain curves for the six different PDMS formulations show that the curves for each type (n = 6) are clustered and separated from the curves of the other formulations, PDMS was cured at 65℃ overnight (12–24 hours) [15]

As mentioned earlier, the mechanical properties of PDMS depend on its mixing ratio. Other than that the curing temperature and curing time of PDMS also affect its mechanical properties [16]. Figure 2.8 indicates how curing temperature affects the stress-strain curve of the PDMS.

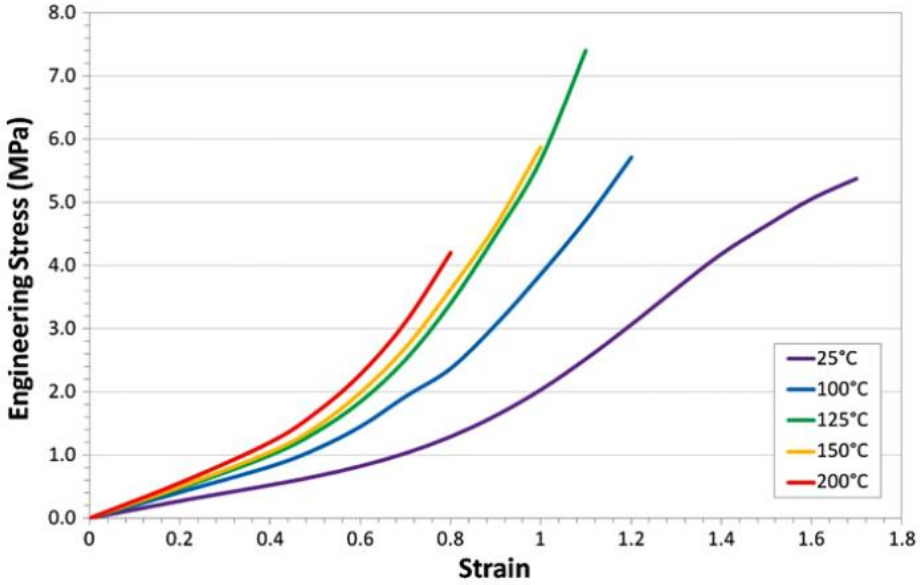


**Figure 2. 8.** Stress-Strain curve for five PDMS samples cured at different temperatures [16]

[3] Slope of the stress-strain curve indicates the modulus of elasticity of the material.

The PDMS as a polymer can be classified in the category of hyperelastic materials, in which the strains may be large. To describe this hyperelastic behavior, the strain energy density function is developed in the aforementioned form. Several different strain energy density functions have been proposed and most of them are in the same described format such as Neo-Hookean, Mooney-Rivlin and Ogden models.

# 3. RESEARCH METHODS AND MATERIALS

This chapter contains the research methods applied to obtain the results. To achieve the desired results, three different design concepts for the structures are developed. The three designed structures are studied separately using a finite element computational model and the results are provided in the following chapter. Methods to implement the computational model of the problem in COMSOL Multiphysics 5.1 software are discussed. Methodological approach to define objective functions required for optimization is also described in this chapter.

## 3.1. Conceptual Design

In order to take steps beyond state of the art, the previously designed structure has been modified to switch the device operation from equiaxial stretching into unidirectional stretching. The common base structure has been introduced in State of the Art Section of the introduction chapter.

The new geometry involves rigid parts which are designed to restrict the displacement of PDMS in a manner that provides a unidirectional strain field within the area under study. The basic idea is to design the cover plate so that it confines the displacement of the PDMS part in a certain axis. Restriction of displacement along an axis and allowing displacement in a perpendicular axis will result in a unidirectional strain field on the surface.

To achieve the goal i.e. unidirectional stretching of cells, three different geometries for the rigid parts of the cover plates are proposed and each is studied separately by means of numerical simulation using COMSOL Multiphysics 5.1 as simulation software.

The first proposed geometry contains a cover plate with circular rigid parts. The second geometry involves rigid parts which are designed according to geometry definition of an ellipsoid. The third geometry includes rectangular rigid parts.

### 3.1.1. Circular Design

The first designed geometry of the rigid parts is a circular geometry. In this case, the important parameters to study are the length of the arc and the height of the rigid parts. The other parameters studied were related to PDMS common base structure and includes the gap size between the PDMS rings and the thickness of inner cylindrical shell. These are selected based on test simulations carried out to identify the parameters with major effect on stress-strain results. Figure 3.1 illustrates the circular design.

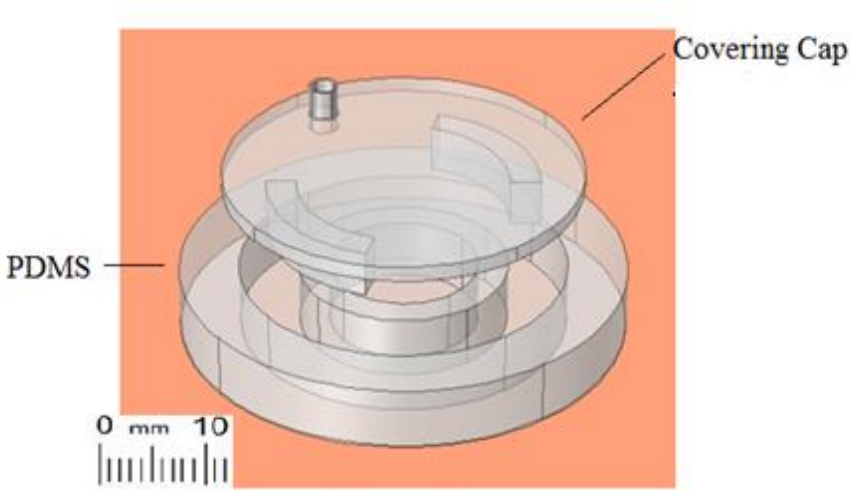


**Figure 3. 1.** Circular design concept for the rigid parts

Figure 3.2 indicates a quarter cut model of the structure and the geometric parameters: the arc length of the rigid parts (b), the height of the rigid parts (h), the gap size between the PDMS rings (g), and the thickness of the inner cylindrical shell (t). The initial geometric parameters of the structure to be studied were chosen to be t=2 mm, g=3 mm, h=5. 9 mm and b=6 mm. The gap between the inner cylindrical shell and the rigid parts was chosen to be fixed at 0.1 mm.

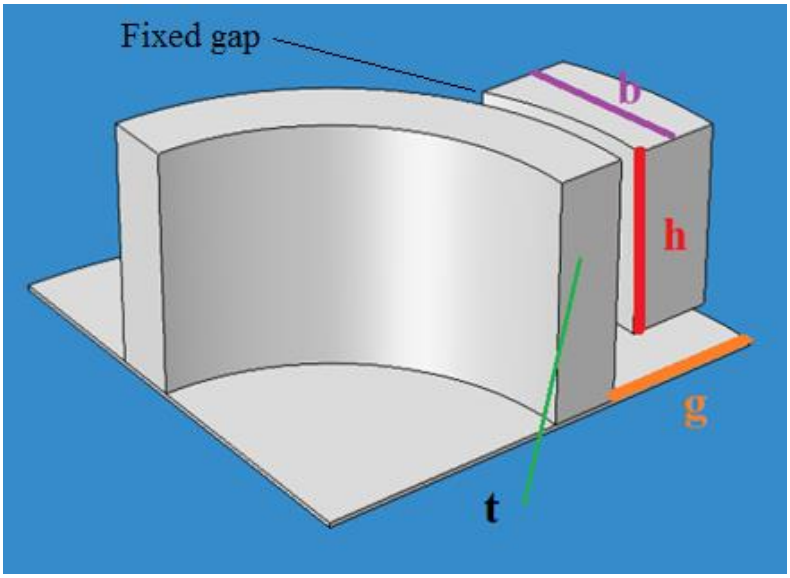


**Figure 3. 2.** Geometric parameters of the structure; t, b, g, and h

### 3.1.2. Rectangular Design

The second geometry possesses rectangular rigid parts as the displacement restrictor. In this case the length of rectangular rigid parts does not have any major effects on final results as long as the distance of the PDMS ring and rigid parts increases when receding from center line. Thus, when PDMS is deformed under applied vacuum pressure, it does not make contact with rigid parts in areas distanced from the middle of the rectangular cube. Therefore, in this case, the studied parameters are the height of the rigid parts (h),

the gap size between the PDMS rings (g), and the thickness of the inner cylindrical shell (t). Figure 3.3 illustrates the rectangular design concept for rigid parts.

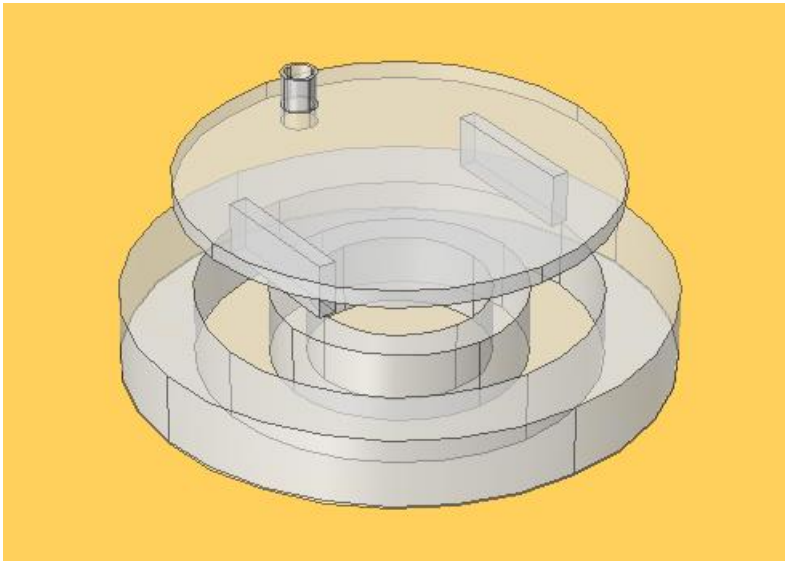

**Figure 3. 3.** Rectangular design concept for the rigid parts

### 3.1.3. Ellipsoidal Design

In the third geometry, the rigid parts are defined by an oval geometry. In an ellipsoidal structure, important parameters to investigate are the semi-major and the semi-minor axes of the ellipse. Figure 3.4 illustrates the ellipsoidal design concept for rigid parts.

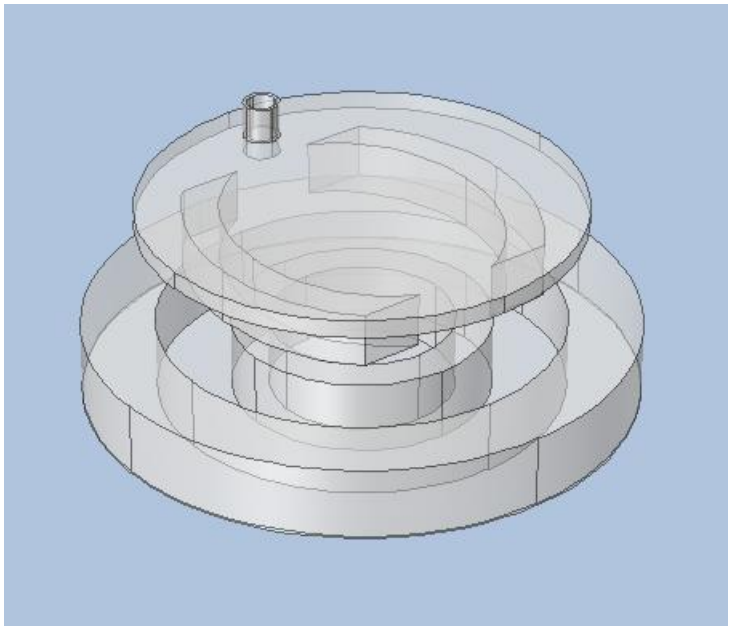

**Figure 3. 4.** Ellipsoidal design concept for the rigid parts

The definition of geometry for oval rigid parts differs from that of circular rigid parts and the geometrical presentation are explained in the following.

In this concept the gap between the inner cylindrical shell and the rigid parts increases from a fixed value at minimum to another value at maximum obeying ellipsoid equation.

In this case the semi-minor value of ellipsoid was fixed to be equal to the sum of the inner ring gap size, and thickness of the inner cylindrical shell. Thus the middle of the rigid parts is in contact with PDMS structure, i.e. distance between them is zero in the middle. The semi-major value was defined to be equal to sum of semi minor value and one changing variable (s). The arc length of the rigid parts, then is determined by a changing variable which defines the polar angle of the angular coordinate (Θ). Figure 3.6 illustrates the geometry definition and geometric parameters.

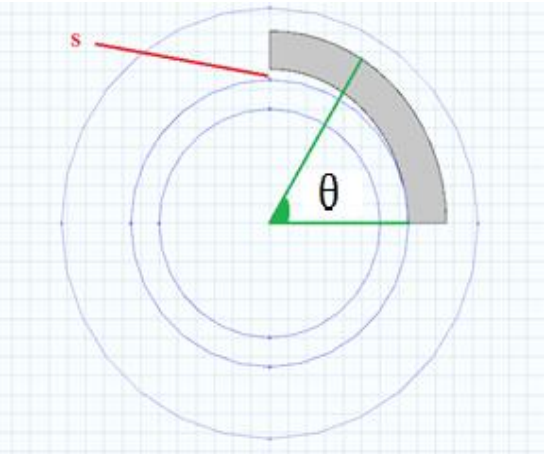


**Figure 3. 5.** Definition of geometrical parameters; s and **Θ**, top view of the design

## 3.2. Computational Modelling using Finite Element Method

This section describes the methods used to construct the computational model of the device and implementation of the model in COMSOL Multiphysics software.

COMSOL Multiphysics is a finite element analysis, solver and Simulation software / FEA Software package for various physics and engineering applications. In our study, the Structural Mechanics Module was used for analysis of structures which were subjected to static pressure loads. The Optimization Module was used in conjunction with Structural Mechanics Module for optimization purpose, taking into account the defined objective functions, design variables, and the constraints.

### 3.2.1. Definition of Material Properties for FE Modeling

According to Fuard et al. [18], the elastic modulus of PDMS could vary from 0.8 MPa to 4 MPa depending on fabrication condition. The Young's modulus of PDMS sample prepared by mixing base and cross-linker with 10:1 weight ratio and cured at 65 ℃ for two hours, is measured to be 2 MPa [11]. PDMS is an incompressible material and the Poisson's ratio for an incompressible material is 0.5. However, in this study the Poisson's ratio is determined as 0.49 for preventing a numerical error in computation. Having Young's modulus and Poisson's ratio determined, other dependent parameters can be calculated.

In this study, Neo-Hookean constitutive material law is designated for the finite element modeling of the hyperelasticity. Neo-Hookean is the simplest approach to model hyperelastic materials, but it is still accurate enough to model applications with small strains (in order of 0.1). As previously mentioned in Section 2.2, for small strains (less than 0.1), the three material models of Linear elastic, NeoHookean, and Mooney-Rivlin, yield the same results (See Figure 2.5). Consequently, the more complex hyperelastic material models with higher order terms which are also more time consuming are not needed. Choosing Neo-Hookean hyperelastic material model, initial bulk modulus ($\kappa$), Lame´ parameter ($\mu$) and density of the material should be determined.

According to equations presented in Section 2.1, the initial bulk modulus is calculated to be equal to $3.333 \times 10^7$Pa and second Lame´ parameter is calculated to be equal to $6.67 \times 10^5\ N/m^2$. The density of PDMS is 971 $kg/m^3$.

The material for rigid parts is designated to be ABS-M30i (Biocompatible Acrylonitrile/Butadiene/Styrene) suitable for 3D printing, with Young's modulus of 2.4 $GPa$ and Poisson's ration of 0.35 and density of 1050 $kg/m^3$ [19].

### 3.2.2. Implementation in COMSOL Multiphysics 5.1

According to symmetric geometry of the structure and in order to minimize the computation time, a quarter model of the structure is simulated. Figure 3.7 indicates the symmetry surfaces in blue.

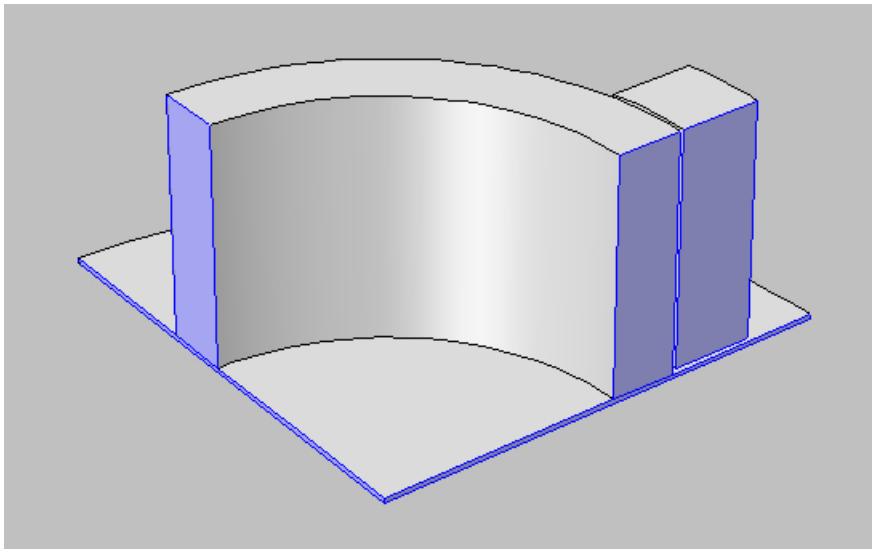

**Figure 3. 6.** Symmetric surfaces of the structure (shown in Blue)

To implement the FEM simulations for this special case in which the two structures, i.e. PDMS and rigid parts, come into contact, contact modeling is required. The contact modeling in COMSOL Multiphysics 5.1 is based on defining a contact pair and determining the source boundaries and destination boundaries. Figure 3.8 illustrates the source boundaries colored in pink and destination boundaries in yellow. Destination boundary is the surface boundary which, despite having contact with the source boundary is fixed and source boundary is a movable boundary.

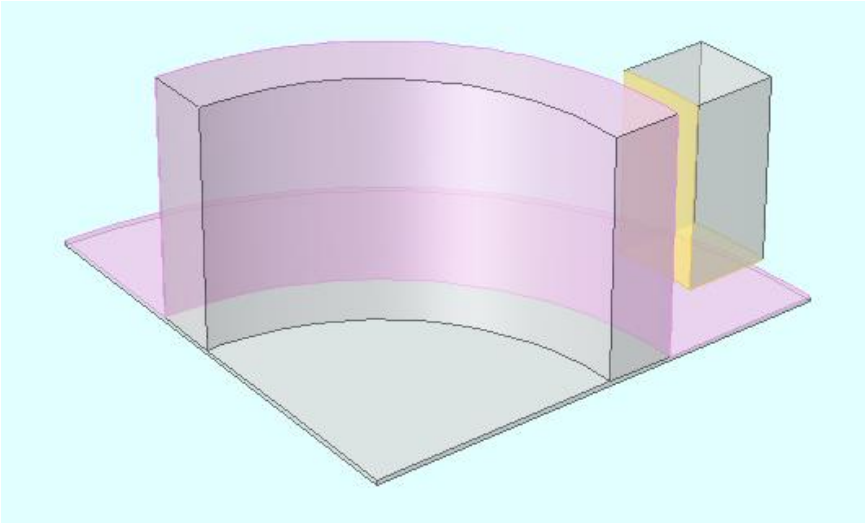

**Figure 3. 7.** Contact pair definition; source boundaries (Pink) and destination boundaries (Yellow)

## 3.3. Defining Objective Function for Optimization

As one of the main purposes of this work is to optimize the structural geometry of the device, optimization module of the software is used in conjunction with the structural mechanics module. The optimization module runs the numerical simulation based on geometric parameters and calculates a predefined objective function in order to compare different geometries.

In order to solve an optimization problem, objective functions are required to be defined. Optimization method and a creative method to define objective functions used in this study are described in the following sections.

### 3.3.1. Optimization Method

The optimization method developed for measuring the unidirectionality is based on the calculation of the fraction of the total area under study, i.e. the surface area where cells are deposited, that satisfies a given condition. For this purpose an integral objective is defined in software environment which calculates the mesh area, taking into account the defined conditions. Monte Carlo optimization solver of COMSOL Multiphysics 5.1 version has been used, which automatically chooses values based on the fact that the objective function varies very randomly when geometry parameters have been changed.

Three different approaches for the objective functions are used in this study. The first approach focuses only on first principal strain. This is only used for test simulations to understand the effects of each geometry parameter on the magnitude and the orientation of the first principal strain. This also allows determining in which range, the geometry parameters are needed to be studied. The second approach provides a more accurate definition of unidirectionality by taking the magnitude of the second principal strain into consideration. The third approach takes into account the uniformity of the provided strain field, as well.

### 3.3.2. Mathematical Expressions for Objective Functions

An objective function is an equation that is required to be optimized, i.e. minimized or maximized. Objective functions include variables and constraints. In this study, the objective function is defined as a surface integral over the area under study, i.e. base membrane surface, with specific predefined conditions. This means that only the regions of the surface area when certain conditions are satisfied are calculated as an expression for objective function.

As mentioned, one of the objectives of this study is achieving unidirectional strain field. The method used to specify unidirectionality is setting a constraint on the angle between the orientation of the first principal strain and the desired direction at each element node. Another goal is to maintain the first principal strain as high as possible. Thus a constraint is also set on the magnitude of the first principal strain at each node. These constraints enable achieving a high strain in a desirable orientation.

The equation expressing the objective function is given below:

$$(p \ \wedge q) \rightarrow \oiint dA \tag{41}$$

Where $p$ and $q$ are conditional statements and the contour integral operator defined on the surface is calculating only the area of the elements where the conditional statements are both true. Therefore, if $p$ and $q$ conditions are valid then the surface area is calculated.

As mentioned earlier, in this study, the conditional statements $p$ and $q$ are defined based on two properties of first principal strain, i.e. magnitude and orientation. This can be implemented in COMSOL Multiphysics 5.1 by defining a surface integral objective over the base membrane surface and choosing values for the limits of the conditional statements.

Three different objective functions based on three different approaches mentioned in the previous section are defined. The first objective function is only used for test simulations. The main difference between the second objective function and the third objective function is that the latter one includes a mathematical term to describe the uniformity of the strain field. The second objective function is defined with a higher value as the constraint for the magnitude of the first principal strain, compared to third objective function. However, the third objective function is defined to optimize the uniformity of the strain field, as well. Defining two objective functions that each emphasizes on a specific aspect of the device performance allows maintaining both high strain value and uniformity. The objective functions are described in the following.

**First Objective Function**

For the first objective function, the limits are chosen as $10\%$ for the first principal strain value and $4.43°$ for the angle between orientation of the first principal strain and the desired direction. Thus, only the area containing the nodes which have the first principal strain of higher than $10\%$ in the magnitude and the deviation less than $4.43°$ compared

to the determined direction of the strain is calculated.[4] These limit values are chosen based on test simulations carried out to study the performance of the device. The effects of different limit values on are presented in Figure A2.1 in Appendix 2.

The mathematical equation of Objective Function 1 is:

$$OF_1 = \oiint \big((\varepsilon_1 > 0.1) * (Cos\,(n,V) > 0.997)\big)\, dA \tag{42}$$

The expressions in the parenthesis indicate the conditions of the integral operator. If this equation is divided by the total area of the surface, then it indicates the percentage of the total area that satisfies those conditions. This objective function has been used to study the effects of each individual parameter on first principal strain.

**Second Objective Function**

The second objective function includes a constraint on the magnitude of the second principal strain in addition to previous constraints. Another conditional statement is added to take into account also the second principal strain value at nodes. The second principal strain is desired to be minimized in order to achieve a more unidirectional strain field. This objective function provides more accurate interpretation of our target which is attaining unidirectional strain field. This limit is chosen to be $2\%$. This means the area of elements which have the first principal strain of higher than $10\%$ in magnitude and deviation of less than $4.43°$ from determined direction of the strain, and also the second principal strain of lower than $2\%$ in magnitude, is calculated as objective function. This indicates a first principal strain of at least five times higher than the second principal strain in the measured area. The mathematical equation of Objective Function 2 is given in equation 46.

$$OF_2 = \oiint \big((\varepsilon_1 > 0.1) * (Cos\,(n,V) > 0.997) * (\varepsilon_2 < 0.02)\big)\, dA \tag{43}$$

The expressions in the parenthesis indicate the conditions of the integral operator. This equation is then divided by the total area of the surface which then indicates the fraction of total area that satisfies those conditions which is a more sensible parameter.

**Third Objective Function**

Another important property of this cell-stretching device should be the ability to provide a uniform strain field in addition to all previously mentioned properties. To take into account the uniformity of the strain field, standard deviation[5] of magnitude of first prin-

[4] COMSOL Multiphysics 5.1 directly calculates the cosine value of the angle between the orientation of first principal strain and defined unidirectionality direction. The cosine value was chosen to be 0.997 which is equal to $4.43°$.

[5] Standard deviation ($\sigma$) denotes the amount of variation or dispersion in a set of data values. A lower standard deviation, i.e. closer to 0, demonstrates that the data points are closer to the mean value of the set, and a higher standard deviation proves that data points are spread over a wider range of values. Standard deviation is obtained by the equation below:

cipal strains of nodal elements is considered to be a good tool. The lower standard deviation is identical to a more uniform distribution of strain. Therefore, the standard deviation is a secondary objective function which the aim of this study is to minimize it to reach a more uniform strain field.

As discussed, the two objective functions of the problem are the previously described surface integral with certain conditions and the standard deviation which is an interpretation for uniformity. The aim of this study is to maximize the area that fulfills the predefined conditions and minimize the standard deviation. In order to solve this multiple objective function problem, one solution would be to combine the objective function in integral format and the standard deviation to represent both objectives in one equation.

The objective function should be in the following form since an increase in the numerator and also a decrease in the denominator results in increasing the objective function. Thus the new objective function is designed not only to provide maximized unidirectional strain, but also to serve a uniform distribution of the strain by means of minimizing standard deviation.

$$OF_{new} = \frac{Maximization\ OF}{Minimization\ OF} \tag{44}$$

This objective function is just a mathematical expression and does not have any physical significance unlike the previous ones which represented the area. This takes into account first principal strain magnitude and orientation, second principal strain magnitude and strain field uniformity.

$$OF_3 = \frac{\oint\oint\left((\varepsilon_1 > 0.08) * (Cos\ (n,V) > 0.997) * (\varepsilon_2 < 0.02)\right)\ dA}{\sqrt{\frac{1}{N}\sum_{i=1}^{N}\left(\varepsilon_{1_i} - \bar{\varepsilon_1}\right)^2}} \tag{45}$$

$N$ is the number of elements.

## 3.4. Methods to Analyze Base Membrane

In order to have a more realistic and more accurate presentation of the results, instead of the total area of the surface of the membrane, the area with 1mm distance from the edges of the membrane has been considered due to possible computational error at edges. Figure 3.9 illustrates the selection of the area under study; a circle with a radius of 5 mm centered at the center of the membrane.

---

$\sigma = \sqrt{\frac{1}{N}\sum_{i=1}^{N}(x_i - \bar{x})^2}$ , $\bar{x} = \frac{1}{N}\sum_{i=1}^{N} x_i$

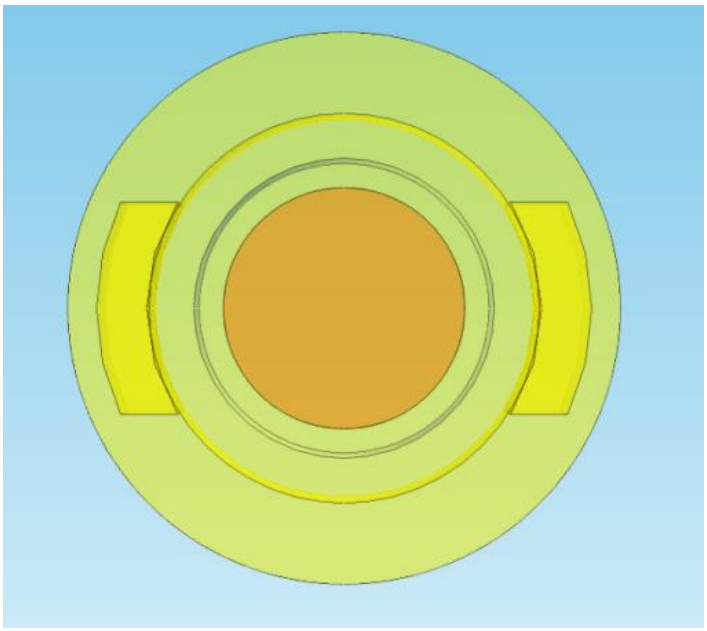

**Figure 3. 8.** Area under study (shown in orange)

The membrane is studied while it experiences deformation under applied vacuum pressure of 36 kPa for uniaxial stretching and 40 kPa for equiaxial stretching. The results are provided in Chapter 4.

# 4. RESULTS AND DISCUSSION

In this chapter, the results of the computational model of the device are provided and discussed. Due to the large number of performed simulations, the data acquired from simulations are given in Tables A1.1-A1.4 in Appendix 1.

## 4.1. Circular Rigid Parts Structure and Effects of Geometric Parameters on First Principal Strain (1st Objective Function)

The first case which was studied was the circular design. In order to reach a better understanding of the influence of the geometric parameters on objective function, the effects of each parameter on the objective function is studied individually. The simulation data is exported and then plotted in MATLAB. The best polynomial curve is fitted to the data using Curve Fitting Toolbox of MATLAB.

Figures 4.1-4.3 and Figure 4.5 present the calculated first objective function when an individual geometric parameter varies while the others are kept constant. Figures are illustrated for the length of the rigid parts (b), the thickness of inner cylindrical shell (t), the gap size between the PDMS rings (g) and the height of the rigid parts (h). The initial geometric values for each case are fixed to be b=6 mm, t=2 mm, g=3 mm and h=5.9 mm. Another geometry parameter that was studied was the thickness of the base membrane. The range in which the thickness of the base membrane was effective on the results had a very limited span (See Figure 4.6). Thus the thickness of the base membrane was not studied in further simulations.

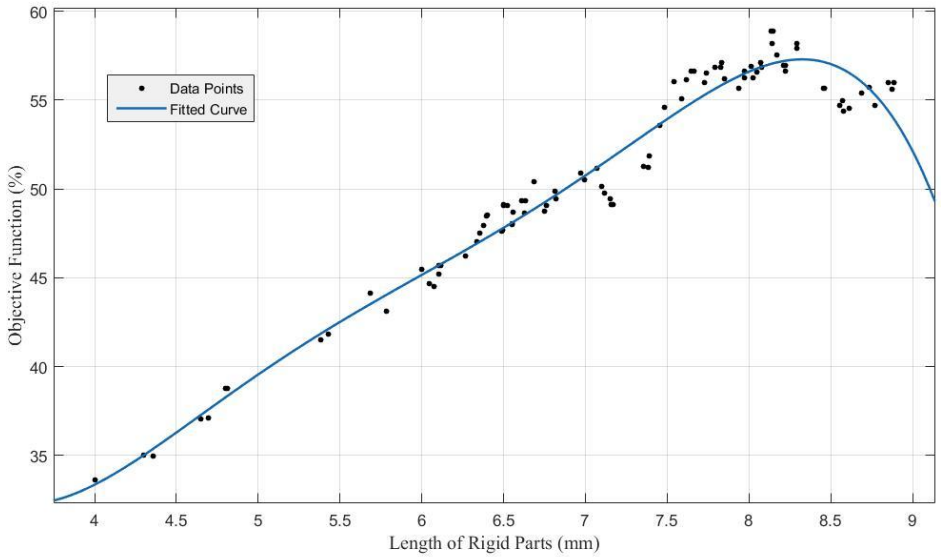


**Figure 4. 1.** First O.F (%) Vs. Length of the rigid parts (mm)

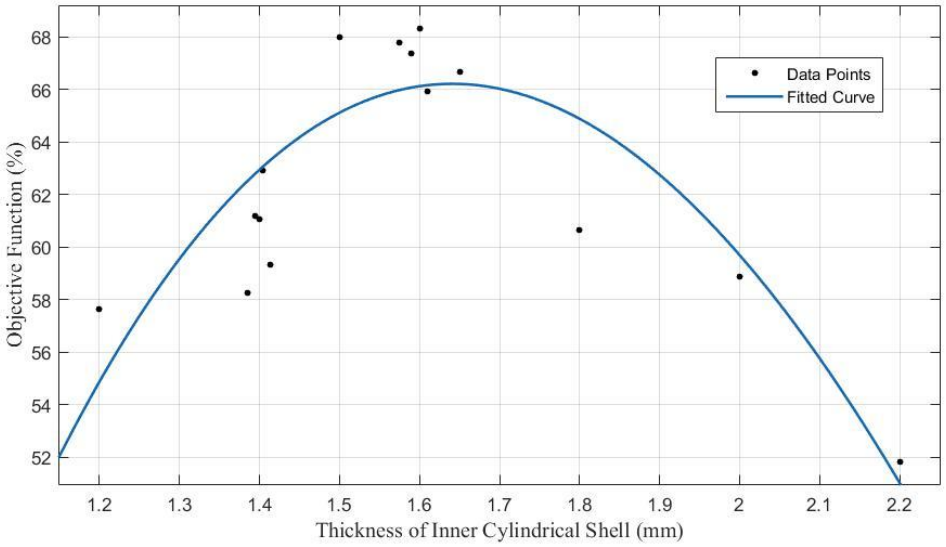


**Figure 4. 2.** First O.F (%) Vs. Thickness of inner cylindrical shell (mm)

These graphs provide us information on the range in which these parameters should be studied. Before executing final simulations while several geometric parameters are varying simultaneously, the varying range of these parameters needs to be specified. Obtaining the maximum of the fitted curve in this specific range describes that the study range is well defined. It can be seen through Figures 4.2-4.4, that the maximum of the fitted curves sits within the studied ranges. This ensures that the study range of these geometric parameters is correctly determined.

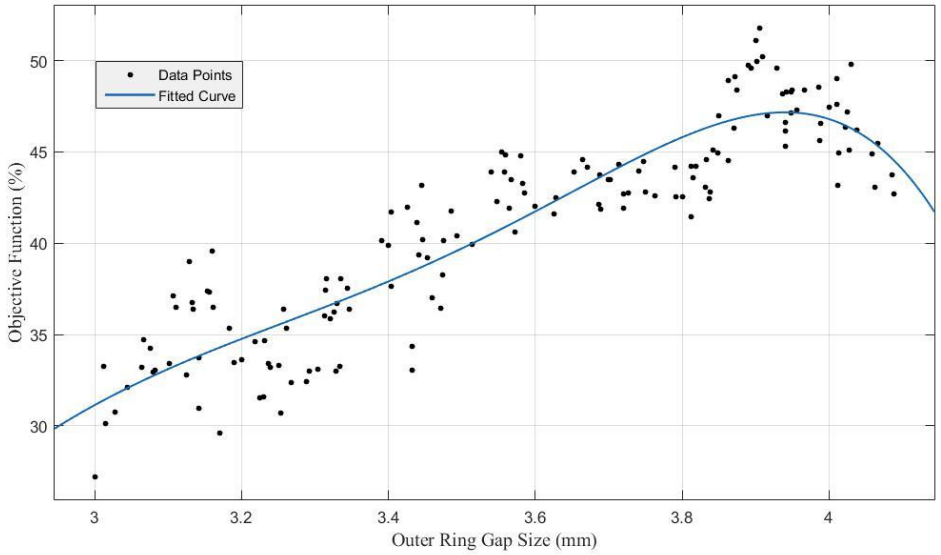


**Figure 4. 3.** First O.F (%) Vs. Gap size between the PDMS rings (Outer Ring Gap Size) (mm)

Figure 4.4 indicates the impact of three aforementioned parameters on the first objective function while the parameters are varied simultaneously in a 3D graph. The color bar represents the first objective function. The graph is sketched to provide a visual representation of the acquired data from numerical simulations. This 3D graph visualizes the effect of geometrical parameters on the first objective function.

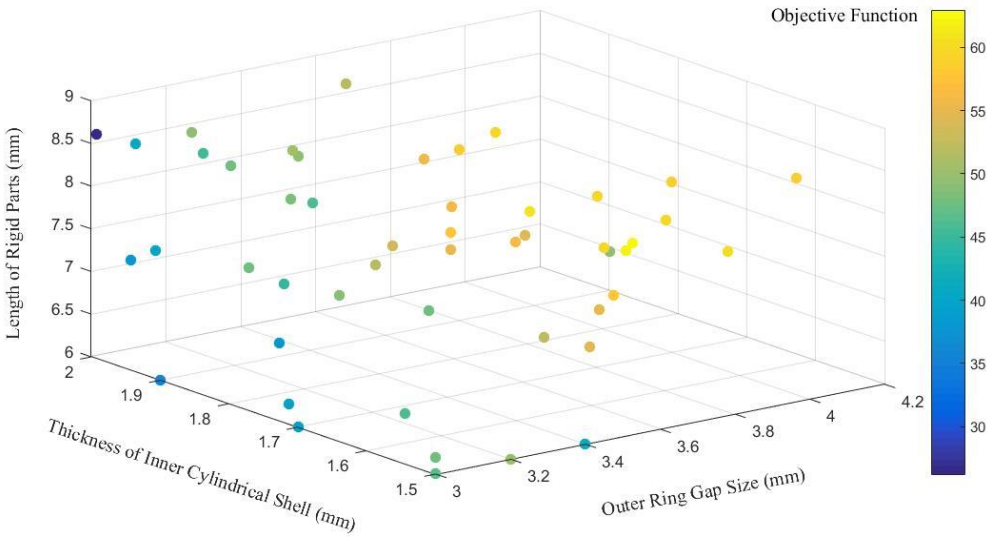


**Figure 4. 4.** First O.F (%) Vs. Length of the rigid parts (mm), Thickness of inner cylindrical shell (mm), and Gap size between the PDMS rings (Outer Ring Gap Size) (mm). (Height of the rigid part = 5.9 mm and Thickness of the base membrane = 0.12 mm)

The two other parameters that are studied are the height of the rigid parts and the thickness of base membrane. Figures 4.5 and 4.6 illustrate how the change in each individual parameter affects the objective function while other parameters are constant. As mentioned earlier, the initial geometric values for each case were fixed to be t=2 mm, g=3 mm and b=6 mm.

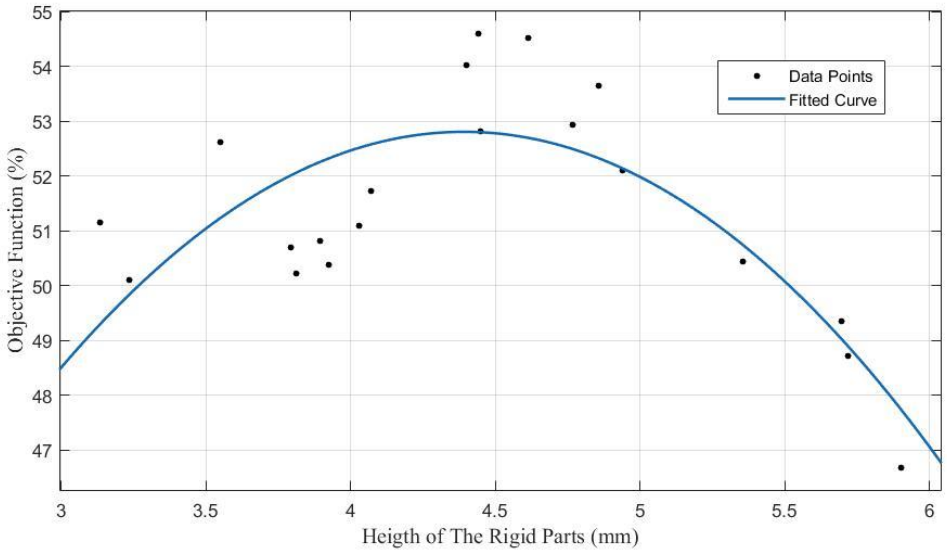


**Figure 4. 5.** First O.F (%) Vs. Height of the rigid parts

Height of the rigid parts as shown in Figure 4.5 have a considerable effect on the objective function and thus was studied as one variable in further simulations.

As indicated in Figure 4.6, the thickness of the membrane is a very sensitive parameter with a very limited length span which is allowed to be varied in. It is clear that increasing the thickness of the base membrane will result in less deformation. Thus the magnitude of strain field on the membrane is confined: for thickness values of higher than 0.15 mm the objective function decreases dramatically until reaches zero level. This parameter is then set out of the parameters to be studied and kept constant at 120 microns.

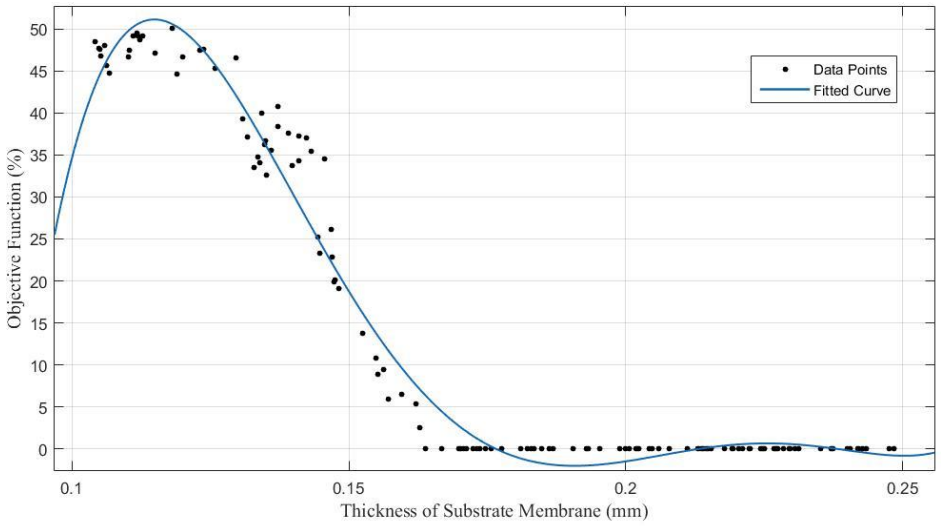


**Figure 4. 6.** First O.F (%) Vs. Thickness of the base membrane

Next, the impacts of all four previously described parameters were studied. The results for first objective function are given in Table 1 of Appendix 1. Results are obtained from simulations with four geometric parameters as input variable. The input values of variables are chosen automatically by COMSOL Multiphysics 5.1 Monte Carlo optimization solver. In this case the maximum value obtained for first objective function was 79.71% for t=1.71 mm, b=8.63 mm, g=4.06 mm and h=3.85 mm.

## 4.2. Different Designs of Rigid Parts and Computational Modelling Results

As discussed earlier, three different designs for structure of rigid parts are studied and the results are provided in Tables A1.1-A1.4 in Appendix 1.

The first design structure is circular rigid parts. The results of the simulations calculating the second objective function, with four changing input variables, i.e. the length of the rigid parts (b), the thickness of inner cylindrical shell (t), the gap size between the PDMS rings (g) and the height of the rigid parts (h), are presented in Table 2 of Appendix 1. The input values are chosen automatically by the optimization solver of the software. The maximum value obtained for second objective function was 57% for t=1.8 mm, b=8.45 mm, g=3.65 mm and h=5.90 mm.

Another proposed structure was a design containing rectangular rigid parts. The results of simulations for this particular design, using the second objective function are pre-

sented in Table 3 of Appendix 1. As it is demonstrated the rectangular design exhibits a very poor performance and thus eliminated as nominee of the final structures.

The third assembly is designing the rigid parts using an ellipsoidal geometry instead of a circle. The results of this set of simulations using the third objective function are given in Table 4 in the Appendix 1. The maximum value obtained for second objective function was 54.50% for t=1.78 mm, b=8.49 mm, g=3.63 mm and h=5.90 mm.

## 4.3. Analysis of the accepted structures

In this section, two of the structures which provided the most satisfying results according to requirements are introduced. One structure with circular rigid parts and the other with oval rigid parts that best satisfy the requirements are studied in detail.

### 4.3.1. Circular Structure

The geometric parameters of the structure that provides the most satisfying performance according to requirements are given in Table 4.1.

**Table 4. 1.** Dimensions of the selected structure with circular rigid parts

| **Geometric parameter** | **t (mm)** | **g (mm)** | **h (mm)** | **b (mm)** |
|---|---|---|---|---|
| **Value** | 1.8 | 3.65 | 5.9 | 8.5 |

**Uniaxial Stretching with Circular Rigid Parts**

The results of the computational model of the device with these geometric parameters are illustrated in Figures 4.7-4.12.

Figure 4.7 presents the displacement of the structure and deformation of the device under applied vacuum pressure of 36 kPa. It indicates how the device is deformed in case of uniaxial stretching. The maximum displacement is 1.47 mm.

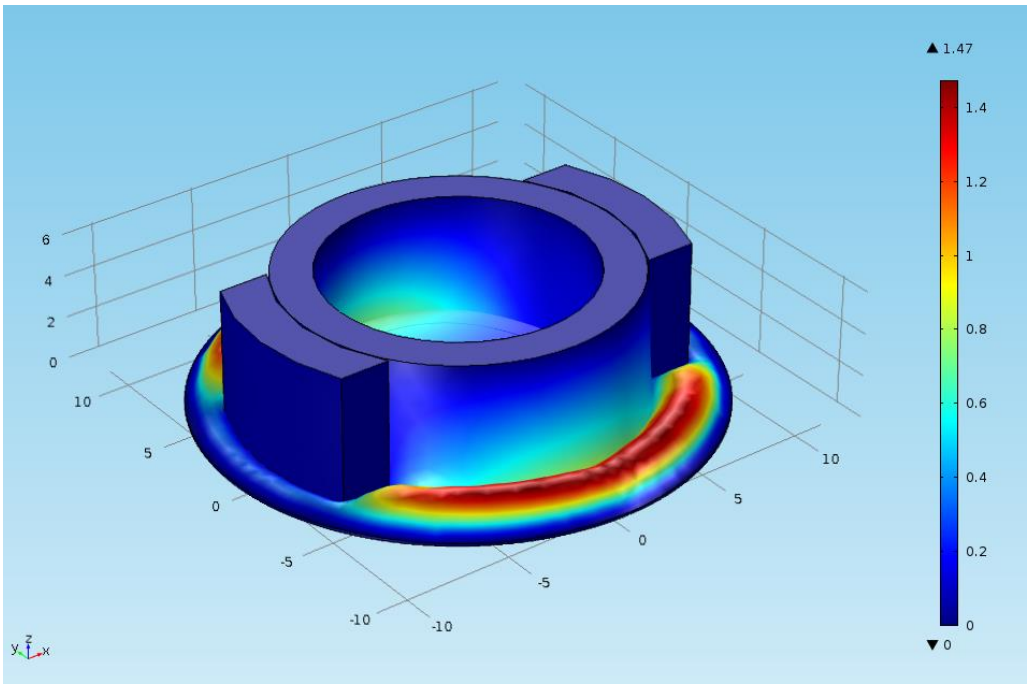


**Figure 4. 5.** Displacement of the structure (mm); uniaxial stretching (Pressure: 36 kPa), circular structure

Figure 4.8 illustrates the first principal strain on membrane surface, i.e. the area where cells are located while Figure 4.9 is illustrated to indicate the second principal strain. The first principal strain is obtained in the range of 7.44%-13.5%. The maximum of the first principal strain occurs in the center of the membrane.

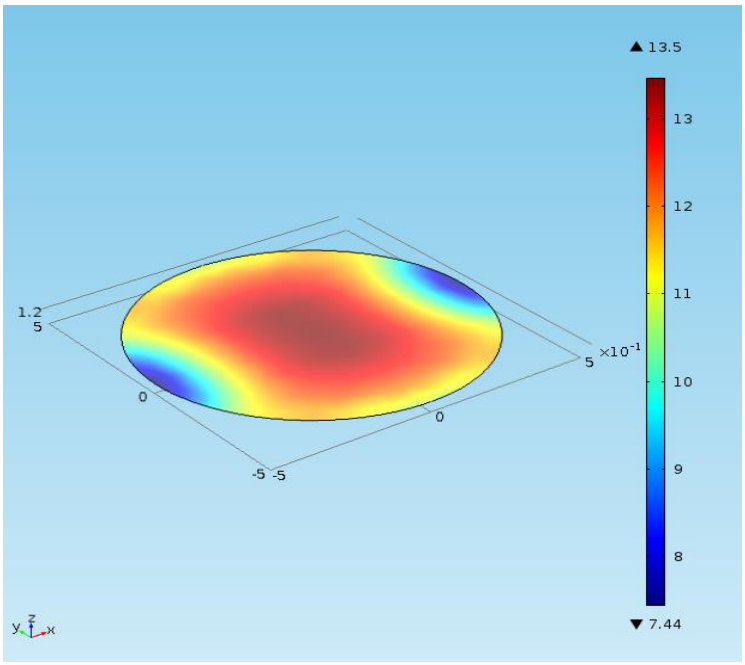


**Figure 4. 6.** First principal Strain (%) on the membrane's surface, uniaxial stretching, circular structure

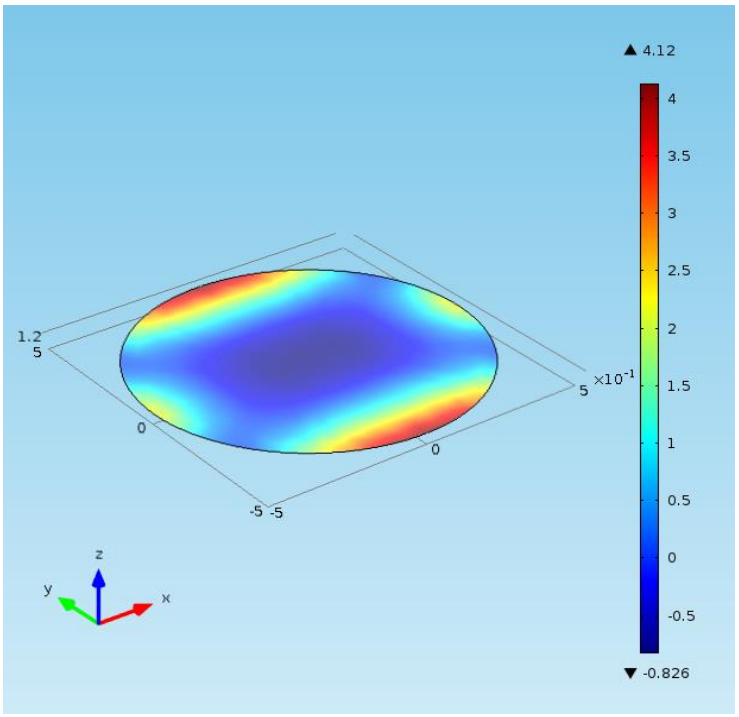


**Figure 4. 7.** Second principal strain (%) on the membrane's surface, uniaxial stretching, circular structure

Figure 4.9 indicates the obtained value for the second principal strain on the surface of the membrane. In the central areas of the membrane, the value is below 2%.

Figure 4.10 presents the degree value of the angle between the first principal strain and the desired direction which in this case is the Y direction of the defined coordinate system. Only on the edges the obtained value of this angle is larger than 4.43°.

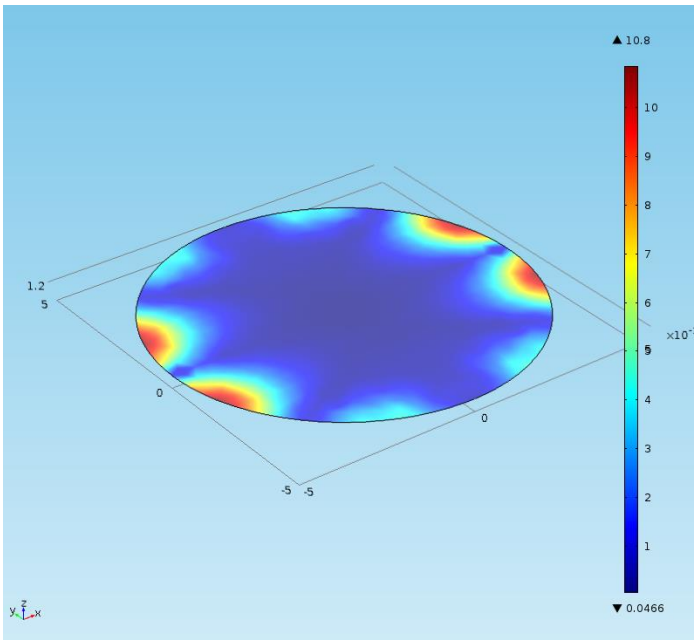


**Figure 4. 8.** Degree value of the angle between the first principal strain and Y direction of the coordinate system, uniaxial stretching, circular structure

Figure 4.11 illustrates the area where predefined conditions for the second objective function are satisfied. Thus, it presents the area that the first principal strain is larger than 10%, the second principal strain is smaller than 2% and the angle between the direction of the first principal strain and the desired direction is less than 4.43°. The 0 value states that the condition is false and 1 value describes that the condition is true.

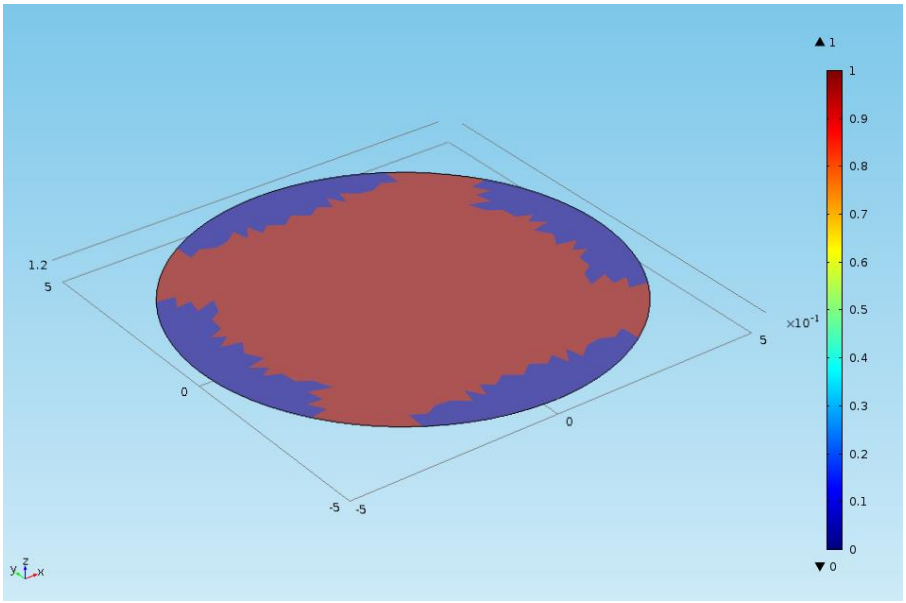


**Figure 4. 9.** Location of the nodes within the area that the first principal strain is larger than **10%**, second principal strain is smaller than **2%**, and the angle between the direction of first principal strain and desired direction is less than **4.43°,** uniaxial stretching, circular structure

Figure 4.12 demonstrates the magnitudes and directions of the principal strains and provides a vector representation of the principal strains on membrane's surface. The red arrows indicate the first principal strain and the green arrows indicate the second principal strain. The lengths of the arrows are proportional to the magnitude of strain.

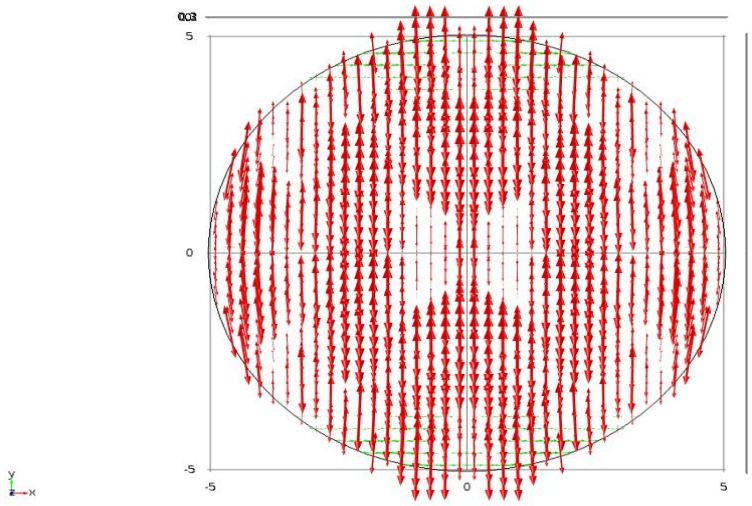


**Figure 4. 10.** Vector representation of the principal strains, uniaxial stretching, circular structure

The surface area that satisfies the defined conditions of having first principal strain over 10% in magnitude, having magnitude second principal strain less than 2% and having the angle between the direction of first principal strain and desired direction less than 4.43°, is 57% of the total area under study, i.e. circle with a radius of 5 mm. The average of first principal strain on whole surface is 11.8%±1.2% and the surface average for the absolute value of second principal strain is 0.9%±1.1%.

**Equiaxial Stretching**

As the idea behind this study is to provide both equiaxial strain and uniaxial strain with one single device, the performance of this structure without applying the cover plate is also simulated. The results of the computational model, is illustrated in Figures 4.13-4.14. Figure 4.13 expresses displacement and deflection of the structure while experiences a vacuum pressure of 40 kPa.

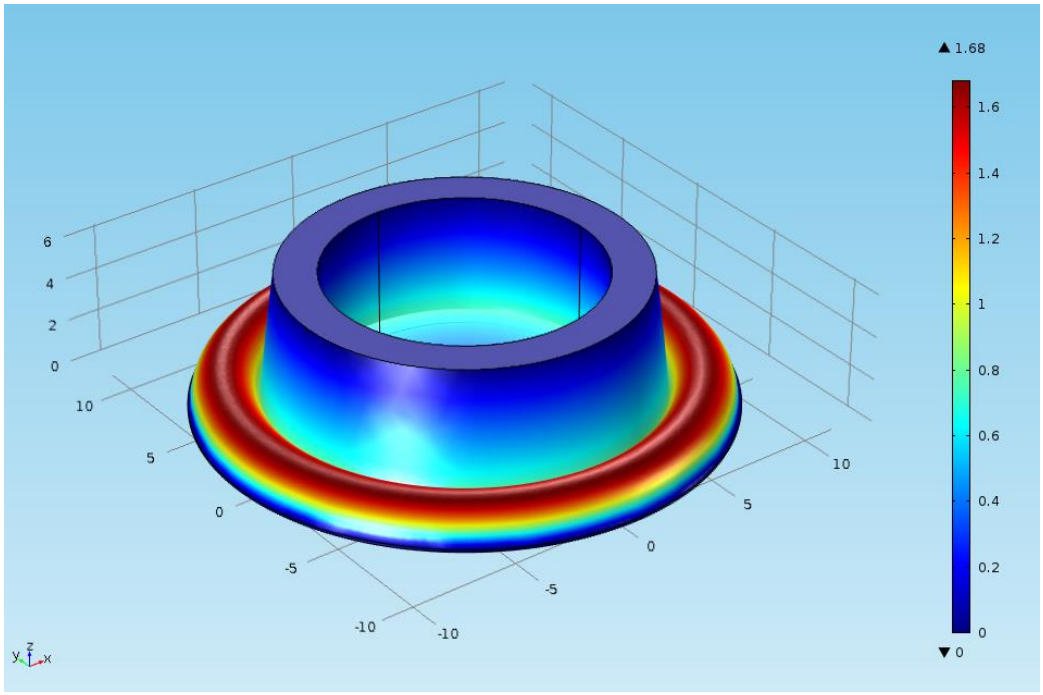


**Figure 4. 11.** Displacement of the structure (mm), eqiiaxial stretching, (Pressure: 40 kPa)

Figure 4.14 indicates first principal strain or second principal strain. The fact that in case of equiaxial stretching the strain should be equal in every direction implies that first principal strain and second principal strain possess a same magnitude. Thus the results are the same for both first and second principal strains in case of equiaxial stretching. The magnitude of the first and second principal strains in case of equiaxial stretching is 12%.

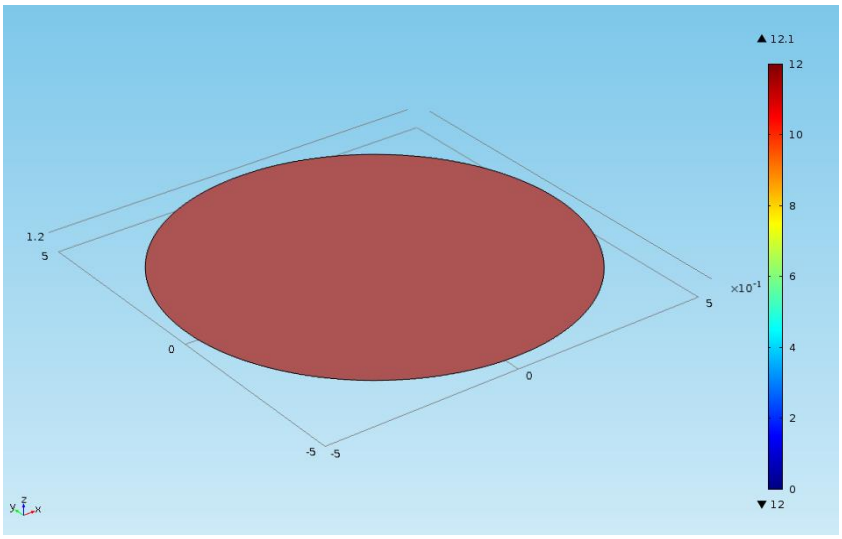


**Figure 4. 12.** First or second principal Strain (%) on the membrane's surface, equiaxial stretching

## 4.3.2. Oval Rigid Part Structure

The geometric parameters of the structure that provides the best performance, according to requirements are given in Table 4.2.

**Table 4. 2.** Dimensions of the selected structure with oval rigid parts

| **Geometric parameter** | **t (mm)** | **g (mm)** | **s (mm)** | **h (mm)** | **θ (degree)** |
|---|---|---|---|---|---|
| **Value** | 2 | 2.6 | 0.6 | 5.25 | 52 |

**Uniaxial Stretching with Oval Rigid Parts**

The same figures as for the circular structure are provided for the structure with oval rigid parts. Figure 4.15 presents the displacement of the structure under applied pressure of 36 kPa. The first principal strain on the surface of the membrane is provided in Figure 4.16 and Figure 4.17 illustrates the second principal strain on the membrane. Figure 4.18 indicates the degree value of the angle between the first principal strain and Y direction of the coordinate system. The area where predefined conditions for the second objective function are satisfied is presented in Figure 4.19 and the vector representation of the principal strains is illustrated in Figure 4.20.

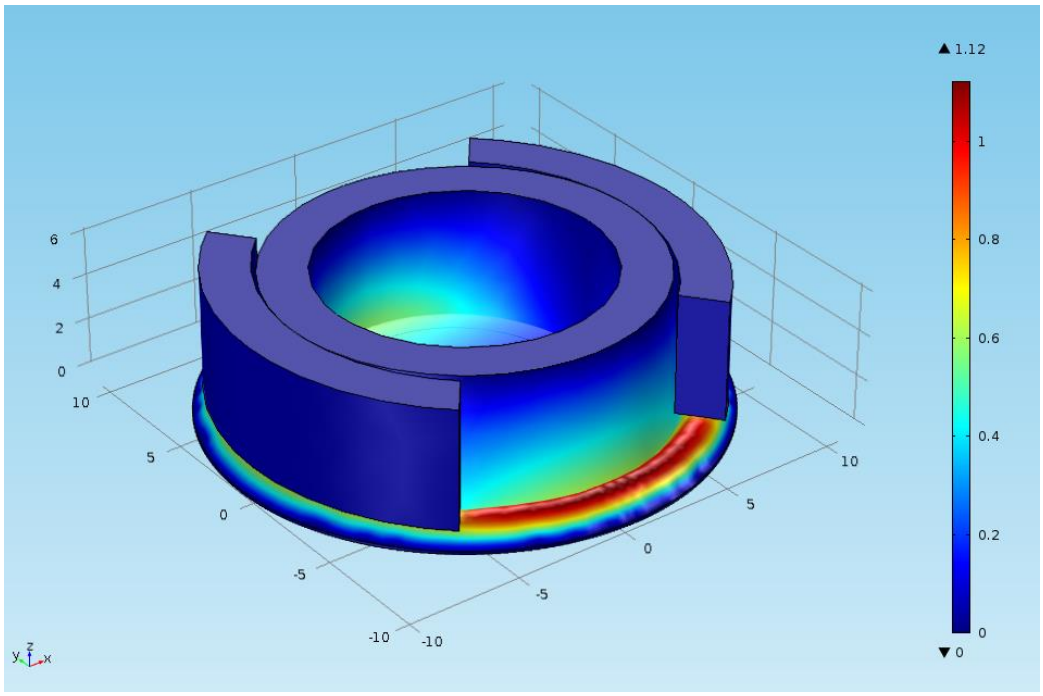


**Figure 4. 13.** Displacement of the structure (mm), uniaxial stretching, oval structure, (Pressure: 36 kPa)

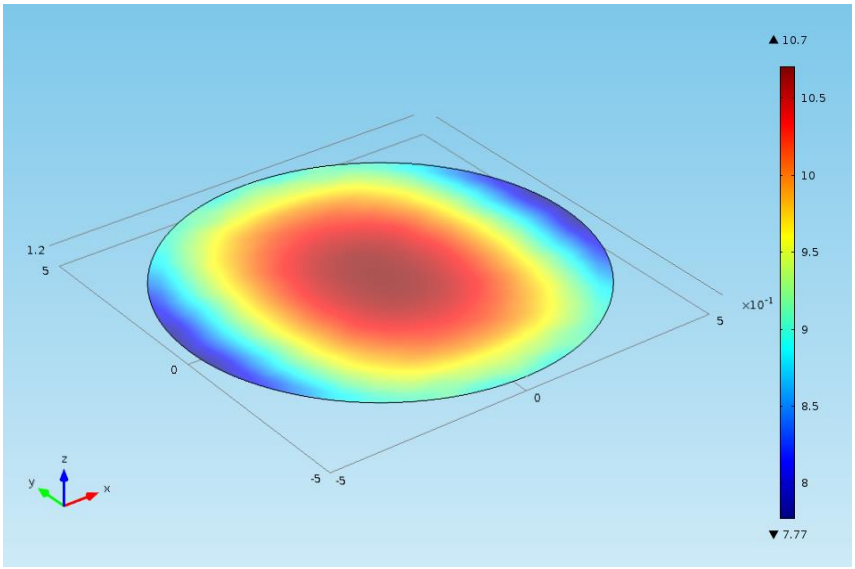


**Figure 4. 14.** First principal Strain (%) on the membrane's surface, uniaxial stretching, oval structure

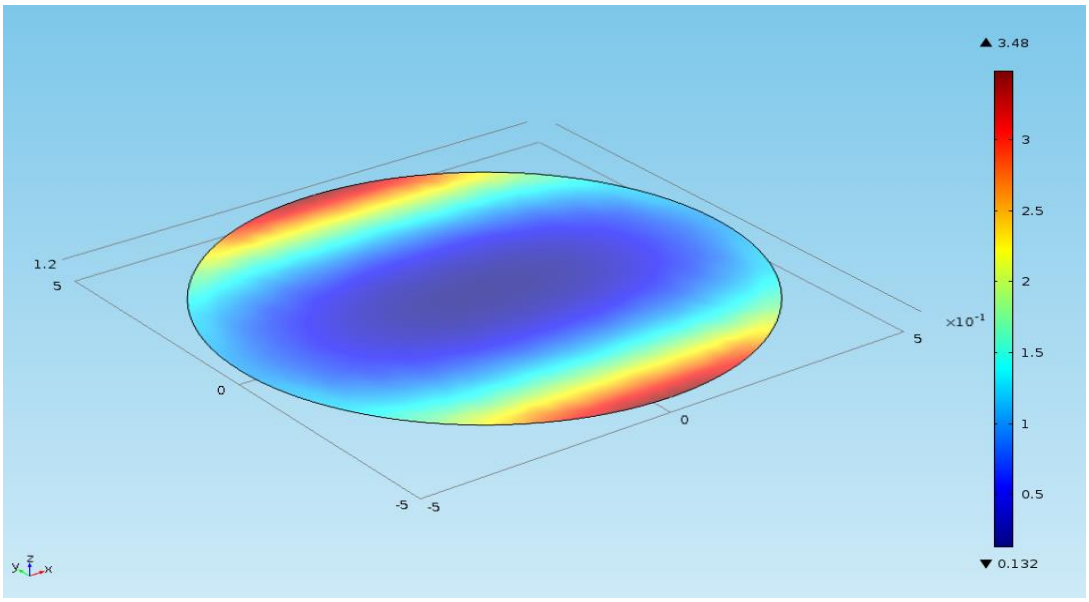


**Figure 4. 15.** Second principal Strain (%) on the membrane's surface, uniaxial stretching, oval structure

The first principal strain is obtained in the range of 7.77%-10.7% and as it can be seen the maximum of the first principal strain occurs in the center of the membrane. The obtained values for the second principal strain on the surface of the membrane are in the range of 0.13%-3.48%. In the central areas of the membrane, the value is below 2%.

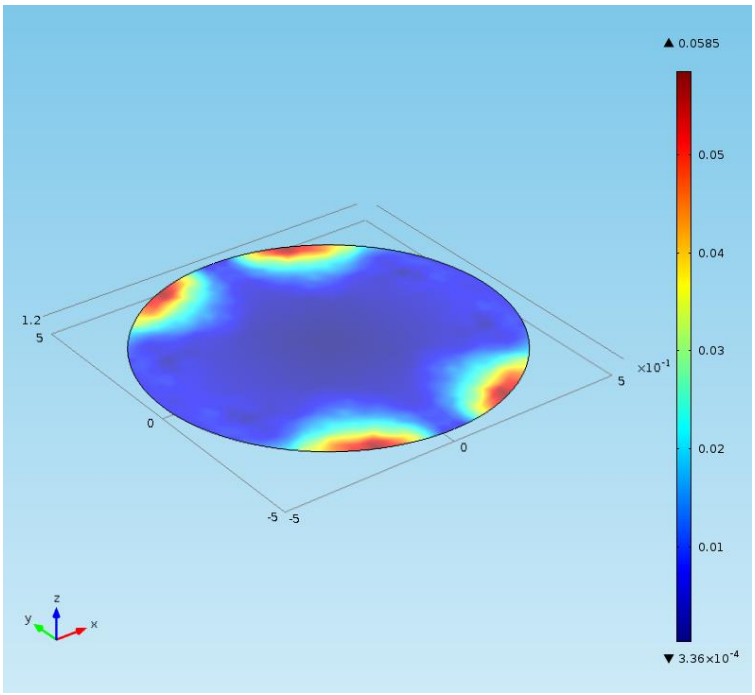


**Figure 4. 16.** Degree value of the angle between the first principal strain and Y direction of the coordinate system, uniaxial stretching, oval structure

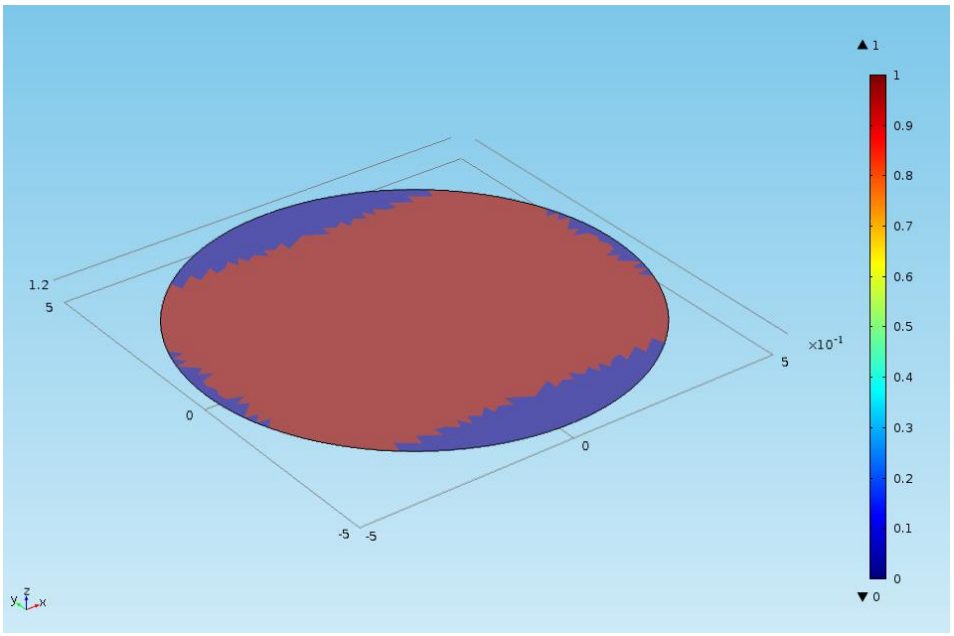


**Figure 4. 17.** Location of the nodes where the area that the first principal strain is larger than **8%**, second principal strain is smaller than **2%**, and the angle between the direction of first principal strain and desired direction is less than **4.43°**, uniaxial stretching, oval structure

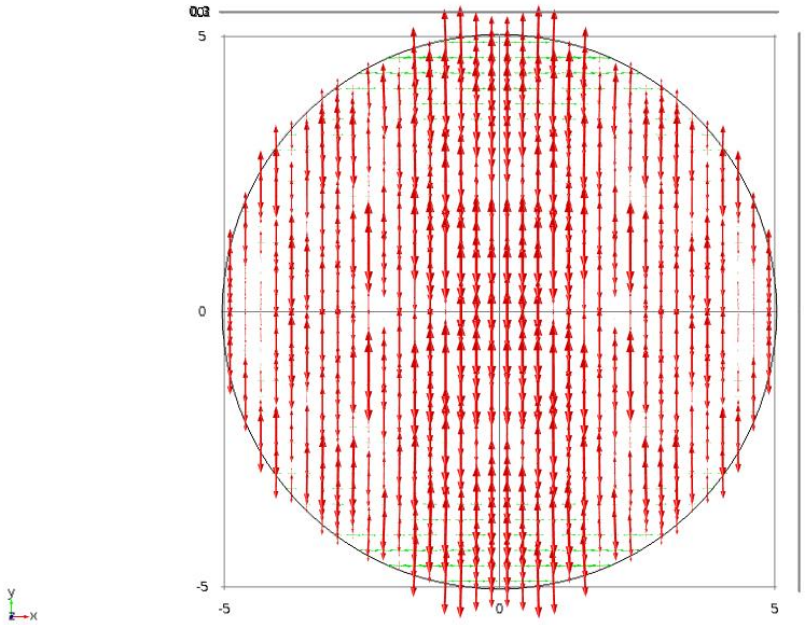


**Figure 4. 18.** Vector representation of the principal strains, uniaxial stretching, oval structure

In this geometry, the surface area that fulfills the predefined conditions of yielding over 8% for magnitude of first principal strain, less than 2% for magnitude of second principal strain, and having the angle between the direction of first principal strain and desired direction less than 4.43°, is 61% of the total area. The average of first principal strain on whole surface is 9.5% and the surface average for the second principal strain is 1.1%.

The standard deviation of first principal strain for total number of nodal elements on the surface is 0.7% for this structure.

**Equiaxial Stretching**

The performance of the oval structure for equiaxial stretching purposes has also been studied and the results for vacuum pressure of 40 kPa are provided. Figure 4.21 represents the displacement and deformation of the structure and Figures 4.22-4.23 which indicate first principal strain and second principal strain respectively, demonstrate that the first and the second principal strain are equal in magnitude. The magnitude of the first and second principal strains in case of equiaxial stretching is 9.7% for this geometry.

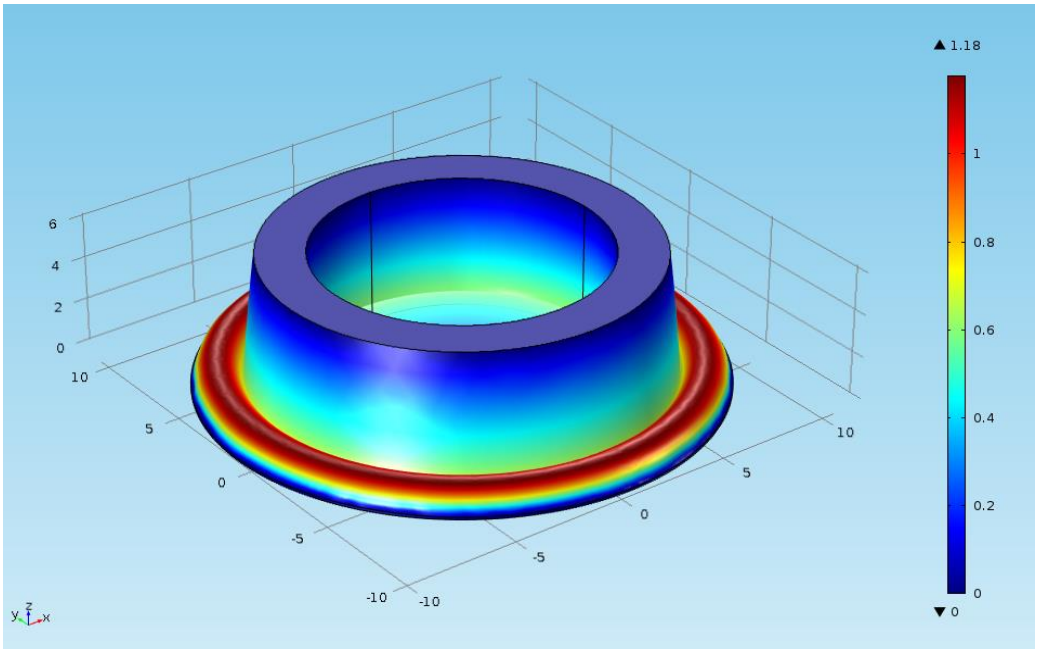


**Figure 4. 19.** Displacement of the structure (mm) (Pressure: 40 kPa), equiaxial stretching

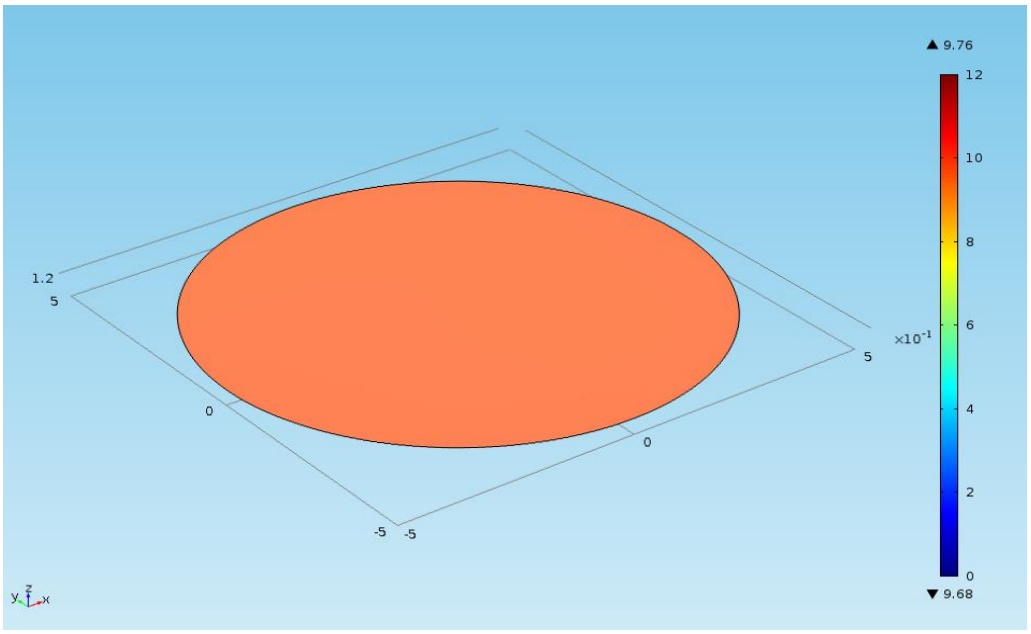


**Figure 4. 20.** First principal strain (%) on the membrane's surface, equiaxial stretching

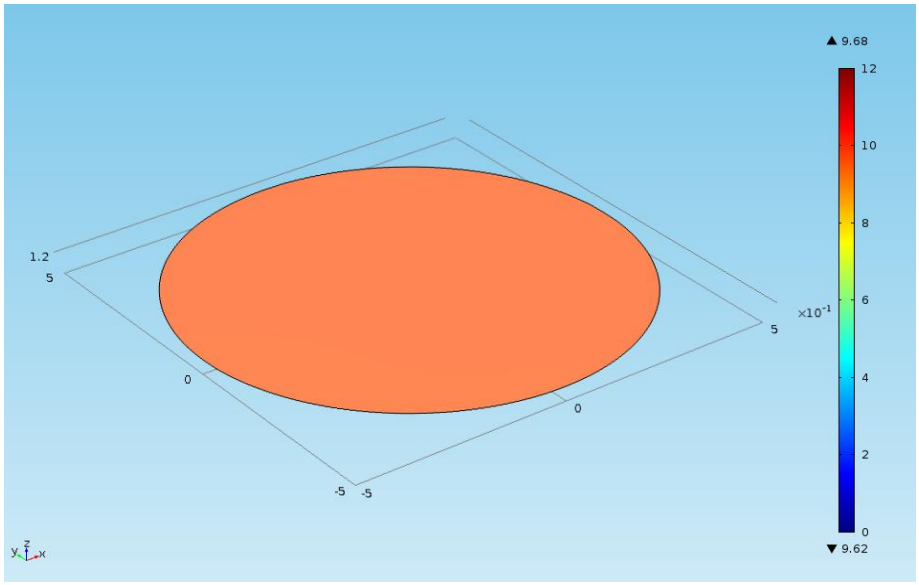


**Figure 4. 21.** Second principal strain (%) on the membrane's surface, equiaxial stretching

## 4.4. Discussion on Results

In this study, to analyze the stress and strain on the membrane, a 1mm distance from the edge of the membrane and the inner cylindrical shell is considered. This was described in Section 3.4 (see Figure 3.9). This was carried out due to possible computational errors in these regions and Figure 4.24 is illustrated to demonstrate that the computational results at the edges are not reliable. As an example, Figure 4.24 indicates that the uniform distribution of the first principal strain in equiaxial stretching mode in the circular structure is varying close to the edges which is not accurate.

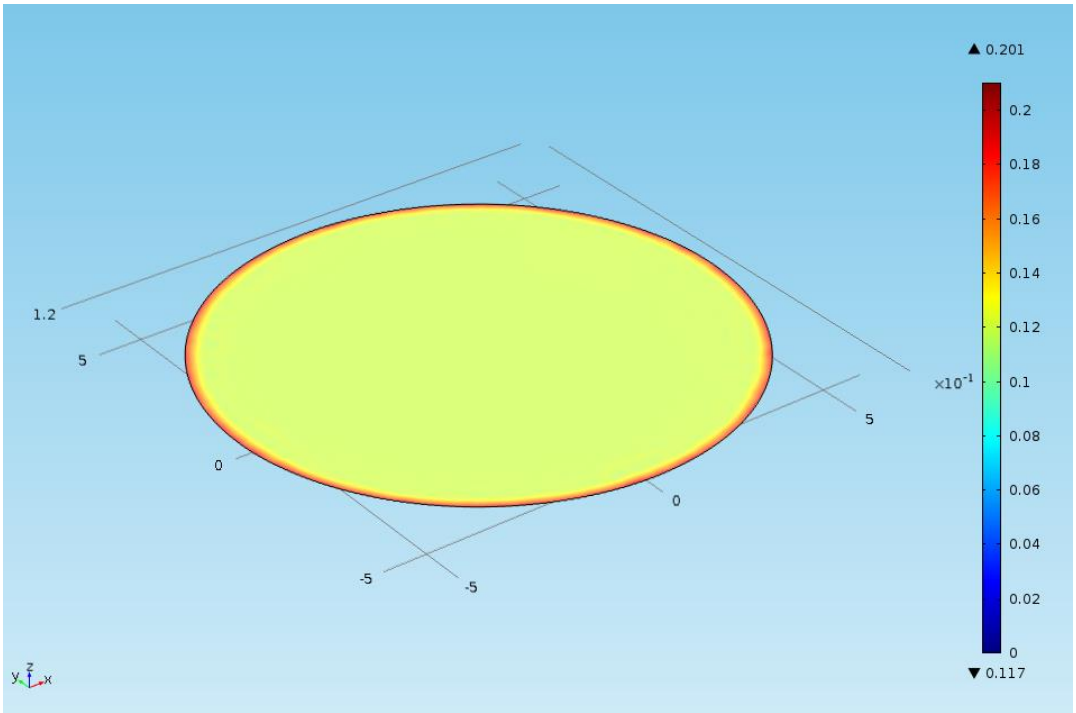


**Figure 4. 22.** First principal strain on the membrane of circular structure in equiaxial stretching mode (radius: 6mm)

The obtained results of numerical simulations imply to be realistic. In case of equiaxial stretching mode of the device, the results are comparable to [11]. Those results have been validated experimentally. The same modelling method has been used to model the device in uniaxial stretching mode and the results accord with logic. Figures 4.9 and 4.18 indicate deformation of the two structures with cover plates comprising of rigid parts under vacuum pressure. It is clear that the rigid parts made of material with relatively high rigidity (E=2.4 GPa) compared to PDMS (E=2 MPa) will not experience a sensible deformation under vacuum pressure of 36kPa and this is obvious in Figures 4.9 and 4.18 in which the deformation of ABS-M30i material is displayed to be negligible. The base membrane which is a thin ($120\mu m$) PDMS layer should experience a large deformation in regions where it is free to deform and this argument perfectly matches the results. As mentioned before, the strain is computed through calculating the displacement field in a deformable body. This whole argumentation implies that the results accommodate with factual performance of the device.

In order to be able to design a single device to provide both uniaxial stretching and equiaxial stretching, a tradeoff between the performances of the device in two different modes of operation is essential. In uniaxial stretching mode, the goal is to obtain the first principal strain as high as possible and the second principal strain as low as possible. In addition to that, the first principal strain field should be as uniform as possible. In equiaxial stretching mode, the goal is to obtain the first principal strain and the second principal strain as high as possible. In this case, the first principal strain and the second principal strain are equal. Other geometrical structures, e.g. ellipsoidal design shape of PDMS rings, might be able to provide a superior performance, according to requirements in case of uniaxial stretching; however this ellipsoidal geometry is unable to produce equiaxial strain. Thus, based on the main idea behind this study, which is to pro-

duce both types of strain fields with one single device using two different cover plates, there must be a compromise in defining the requirements.

This is comprehensible that the circular structure is capable of producing a higher first principal strain and a lower second principal strain. This is justifiable due to the fact that in the case of circular rigid parts, there is a fixed gap size between the rigid parts and inner cylindrical shell which is 100 microns. In contrast, for the case of oval rigid parts the gap is increasing with an ellipsoidal geometric equation from zero value in the middle of rigid parts. This intensifies the restriction of the displacement of the inner cylindrical shell and decreases the magnitude of the first principal strain.

In case of uniaxial stretching, the average values of the first principal strains for circular structure and oval structure are 11.8% and 9.5%, respectively. The surface average of the absolute value of the second principal strain is 0.9% for the circular structure and this value has been obtained to be 1.1% for the oval structure. Thus, in the context of the magnitude of the principal strains, circular structure performs better than the oval structure. As discussed, having the first principal strain as high as possible and the second principal strain as low as possible is desired in case of uniaxial stretching. However the oval structure is capable of producing a more uniform strain field with a standard deviation of 0.7%. The standard deviation of the strain field provided by circular structure is 1.2%. Therefore, in context of uniformity of the distribution of strain field, the oval structure exhibits a preferable performance.

In case of equiaxial stretching, the magnitudes of the first and the second principal strain are 12% for the circular structure and 9.7% for the oval structure. This is noteworthy that in this case the first and the second principal strains are equal and they yield a same value in whole surface.

Afterwards, the decision on which structure to use, has to be made by end user based on whether the uniformity or the magnitude of strain play a more important role in the case.

# 5. CONCLUSION

In this study, a novel design concept for a device capable of providing both uniaxial stretching and equiaxial stretching for cell culturing and stimulation of cells has been proposed. The designed structure provides a relatively good performance, according to defined requirements. Furthermore this pneumatically actuated cell stretching device is simple and easy to fabricate.

To study the performance characteristics of the device, the computational model of the device is implemented in COMSOL Multiphysics 5.1 software. Furthermore, the geometry of the device is optimized to achieve the desired performance. The obtained results for the optimized structure relatively satisfy the objectives of this study.

Although this has been proven that utilizing different types of mechanical stimulation regulates the self-renewal of stem cells and directs their differentiation, but the actual intracellular mechanisms through which the differentiation of stem cells takes place still remains largely unknown. Once these mechanisms are better understood, engineers will be able to design and fabricate more appropriate bioreactors. This includes specially designed cell culture apparatuses aimed to impart an appropriate mechanical force on cells in question while further maintains the appropriate conditions for cell survival. The results of this study are a contribution to this demand. The results of this thesis make it easier to achieve two common forms of cell stretching, i.e. equiaxial stretching and uniaxial stretching with one device. This also reduces the production costs for such apparatuses.

It is concluded that in order to design a single device for equiaxial and uniaxial stretching, a compromise in defining requirements for both cases is necessary. Although, other devices might be able to exhibit a more desirable performance for each individual case, but for this designed device, bifunctionality is a major advantage. Therefore, enabling to achieve the dual purpose of uniaxial and equiaxial cell stretching using one single device, distinguishes this device among other existing devices. In addition to that, the proposed design is easy to fabricate and also transparent. Transparency enables monitoring cells under cultivation on the membrane. This novel design brings advantages that make it unique among other present devices.

The summary of performance characteristics of two different structures for both types of stretching is expressed in the following.

## 5.1. Performance Characteristics of the Devices

This section summarizes the performance characteristics of the two structures in both uniaxial stretching mode and equiaxial stretching mode, respectively. This implies that these two structures provide different performance characteristics. The circular structure provides higher magnitude of strain. The oval structure provides a more uniform strain field, even though the magnitude of strain is smaller.

### 5.1.1. Uniaxial Stretching Mode

For the circular structure, the surface area that satisfies the defined conditions of having first principal strain over 10% in magnitude, having magnitude second principal strain less than 2% and having the angle between the direction of first principal strain and desired direction less than 4.43°, is 57% of the total area under study. In oval structure, the same conditions except for the magnitude of first principal strain which is set to be 8% instead of 10% have been applied and the area that fulfills these conditions is calculated to be 61% of the total are.

The average value of first principal strain on the membrane surface is 11.8% for the circular structure, while for the oval structure this is equal to a smaller value of 9.5%. The surface average for the absolute value of the second principal strain is 0.9% for the circular structure and this value has been obtained to be 1.1% for the oval structure.

The standard deviation of first principal strain for total number of nodal elements on the membrane surface is 1.2% for circular structure. The standard deviation for the elliptic */ or* oval structure is equal to 0.7%.

### 5.1.2. Equiaxial Stretching Mode

The magnitude of the first and second principal strains in case of equiaxial stretching is 12% for the circular geometry and this value is computed to be 9.7% for the oval geometry. This is noteworthy that in this case the first and the second principal strains are equal and they yield a same value in whole surface.

## 5.2. Specifications of the Two Structures

This is comprehensible that the circular structure is capable to produce a higher first principal strain and lower second principal strain in case of uniaxial stretching. In addition to that, it also provides a higher strain in case of equiaxial stretching. Thus, in context of the magnitude of the strain, this structure performs better than the oval structure. However the oval structure is capable of producing a more uniform strain field with a standard deviation of 0.7%. Therefore, in context of uniformity of the distribution of strain field, the oval structure exhibits a preferable performance.

Afterwards, the decision on which structure to use, has to be made by end user based on whether the uniformity or the magnitude of the strain play a more important role in the case.

## 5.3. Future Work

In future, fabrication and experimental validation of the results for optimized structures need to be done. One other possible direction would be to control the performance characteristics of the device by controlling vacuum pressure. It has been noticed that the amount of vacuum pressure applied, highly influences the plane strain and thus the objective function value. This is due to non-linear mechanical behavior of the PDMS. Thus, refining the objective functions and study of the objective functions according to applied vacuum pressure can be investigated. Further optimization of the device by tak-

ing more parameters into account such as the vertical displacement of the membrane can also be done.

# REFERENCES

[1] Stem Cell and Regenerative Medicine, Herman Cheung, 2010, Bentham Science Publishers, ISBN: 978-1-60805-008-6.

[2] Butler DL, Juncosa-Melvin N, Boivin GP, et al. Functional tissue engineering for tendon repair; A multidisciplinary strategy using mesenchymal stem cells, bioscaffolads, and mechanical stimulation. J Orthop Res 2008; 26: 1-9.

[3] Burdick JA, Vunjak-Novakoovic G. Review: Engineered Microenvironments for Controlled Stem Cell Differentiation. Tissue Engineering Part A. July 2009, 15(2): 205-219.

[4] Freed LE, Guilak F, Guo XE, et al. Advanced tools for tissue engineering: scaffolds, bioreactors, and signaling. Tissue Eng 2006; 12:3285-3305.

[5] Wang JH, Thampatty BP. Mechanobiology of adult and stem cells. Int Rev Cell Mol Biol 2008; 271: 301-346.

[6] Estes BT, Gimble JM, Guilak F. Mechanical signals as regulators of stem cell fate. Curr Top Dev Biol 2004; 60: 91-126.

[7] Schmelter M, Ateghang B, Helmig S, et al. Embryonic stem cells utilize reactive oxygen species as transducers of mechanical strain-induced cardiovascular differentiation. FASEB J 2006; 20: 1182-1184.

[8] Sumanasinghe RD, Osborne JA, Loboa EG. Mesenchymal stem cell-seeded collagen matrices for bone repair: effects of cyclic tensile strain, cell density, and media conditions on matrix contraction in vitro. J Biomed Mater Res A 2009; 88: 778-786.

[9] Christine Mummery, Dorien Ward-van, et al. Differentiation of human embryonic stem cells to cardiomyocytes. Journal of the American Heart Association 2003 vol. 107 no. 21 2733-2740.

[10] F. Zhao, J. Kreutzer and P. Kallio, "Computational modeling and structural improvement of a pneumatically actuated concentric double-shell structure for cell stretching," 2014 IEEE International Conference on Mechatronics and Automation, Tianjin, 2014, pp. 906-911.

[11] Zhao, F.; Kreutzer, J.; Pajunen, S.; Kallio, P. Mechanical Analysis of a Pneumatically Actuated Concentric Double-Shell Structure for Cell Stretching. Micromachines 2014, 5, 868-885.

[12] Eshbach's Handbook of Engineering Fundamentals, 5th Edition, Edited by Myer Kutz, 2009, John Wiley & Sons, Inc. ISBN: 978-0-470-08578-3.

[13] Junshan Liu, Guoge Zong, Licheng He, Yangyang Zhang, et al. Effects of Fumed and Mesoporous Silica Nanoparticles on the Properties of Sylgard 184 Polydimethylsiloxane, *Micromachines* 2015, *6*(7), 855-864.

[14] J. Cooper McDonald and George M. Whitesides. Polydimethylsiloxane as a Material for Fabricating Microfluidic Devices, Acc. Chem. Res., 2002, 35 (7), 491–499.

[15] Palchesko RN, Zhang L, Sun Y, Feinberg AW (2012) Development of Polydimethylsiloxane Substrates with Tunable Elastic Modulus to Study Cell Mechanobiology in Muscle and Nerve. PLoS ONE 7(12): e51499. doi:10.1371/journal.pone.0051499

[16] I D Johnston, D K McCluskey, C K L Tan and M C Tracey, Mechanical characterization of bulk Sylgard 184 for microfluidics and microengineering, J. Micromech. Microeng. 24 (2014) 035017 (7pp).

[17] Feihu Zhao, Modelling of Three Dimensional Elastomer Structures for Cell Stimulation using FEM, Master of Science Thesis, Department of Automation Science and Engineering, Tampere University of Technology, 2012.

[18] Fuard, D.; Tzvetkova-Chevolleau, T.; Decossas, S.; Tracqui, P.; Schiavone, P. Optimization of poly-di-methyl-siloxane (PDMS) substrates for studying cellular adhesion and motility. Microelectron. Eng. 2008, 85, 1289–1293.

[19] ABS-M30i material specifications datasheet. [WWW]. [Accessed on 15.07.2016]. Available at: http://www.cimetrixsolutions.com/pdf/material_specs/MS-ABS-M30i.pdf.

[20] Samu Hemmilä, Juan V. Cauich-Rodríguez, Joose Kreutzer, Pasi Kallio. Rapid, simple, and cost-effective treatments to achieve long-term hydrophilic PDMS surfaces, Applied Surface Science, Volume 258, Issue 24, 1 October 2012, Pages 9864–9875

[21] Analysis of Hyperelastic Materials with MECHANICA – Theory and Application Examples, Dr.-Ing. Roland Jakel, PTC Presentation for the 2nd SAXSIM | Technische Universität Chemnitz, 27. April 2010, Rev. 1.0. [WWW]. [Accessed on 15.07.2016]. Available at: http://www.qucosa.de/fileadmin/data/qucosa/documents/5995/data/Analysis_of_Hyperelastic_Materials_with_MECHANICA.pdf.

[22] Samer Adeeb, University of Alberta solid mechanics course textbook. [WWW]. [Accessed on 15.07.2016]. Available at: http://sameradeeb.srv.ualberta.ca/constitutive-laws/hyperelastic-materials/

[23] Dhananjay Bodas, Chantal Khan-Male, Hydrophilization and hydrophobic recovery of PDMS by oxygen plasma and chemical treatment—An SEM investigation, Sensors and Actuators B: Chemical, Volume 123, Issue 1, 10 April 2007, Pages 368–373

[24] David T. Eddington, John P. Puccinelli, David J. Beebe, Thermal aging and reduced hydrophobic recovery of polydimethylsiloxane, Sensors and Actuators B: Chemical, Volume 114, Issue 1, 30 March 2006, Pages 170–172

# APPENDICES

## Appendix 1

**Table A1. 1.** 1st O.F values for input variables; t, b, g, and h, circular rigid part

| t (mm) | b (mm) | g (mm) | h (mm) | 1st O.F |
|---|---|---|---|---|
| 1,6 | 7,8 | 3,7 | 4,5 | 65.6327 |
| 1,9391 | 8,9123 | 4,0029 | 5,1384 | 66.2977 |
| 1,9183 | 7,3134 | 3,1669 | 3,5083 | 4.1572 |
| 1,9024 | 8,376 | 3,006 | 5,3165 | 47.4075 |
| 1,7905 | 7,3763 | 3,6829 | 3,6457 | 62.6972 |
| 1,5739 | 7,9791 | 3,0777 | 5,7914 | 58.7076 |
| 1,9589 | 8,6347 | 3,8128 | 3,4702 | 59.9066 |
| 1,5886 | 6,3038 | 3,1267 | 5,8833 | 50.0035 |
| 1,7538 | 8,6008 | 3,7191 | 4,8608 | 61.6574 |
| 1,7342 | 7,9517 | 3,9384 | 3,7681 | 78.2238 |
| 1,6595 | 7,8589 | 3,2342 | 5,4995 | 59.1957 |
| 1,5319 | 6,8678 | 3,2463 | 4,2384 | 63.0261 |
| 1,8007 | 6,3273 | 3,0514 | 3,913 | 35.7537 |
| 1,6287 | 7,5402 | 3,0414 | 3,6244 | 58.1807 |
| 1,7416 | 7,3949 | 3,8523 | 4,8756 | 74.5844 |
| 1,5022 | 6,0741 | 3,8184 | 4,0797 | 71.0441 |
| 1,5968 | 8,9329 | 3,3718 | 4,8754 | 63.5177 |
| 1,9787 | 6,1407 | 3,3597 | 5,0279 | 39.7538 |
| 1,9554 | 8,1813 | 3,5014 | 4,0429 | 53.6323 |
| 1,563 | 6,802 | 3,3569 | 3,6728 | 74.7436 |
| 1,6172 | 8,511 | 3,2288 | 3,9421 | 70.0396 |
| 1,581 | 7,2095 | 4,0697 | 4,5707 | 69.6010 |
| 1,6416 | 7,0603 | 3,8163 | 5,7236 | 65.1234 |
| 1,6347 | 7,1789 | 3,5228 | 3,4645 | 56.9675 |
| 1,7089 | 8,247 | 3,1153 | 5,7411 | 53.6323 |
| 1,8699 | 6,6386 | 3,4391 | 3,3817 | 35.5521 |
| 1,7944 | 6,1541 | 3,2199 | 3,1296 | 0 |
| 1,7 | 8,65 | 4,05 | 3,85 | 0 |
| 1,5522 | 8,4431 | 3,3414 | 5,4143 | 40.9422 |
| 1,7232 | 9,6995 | 3,3464 | 4,2313 | 0 |
| 1,7542 | 7,0976 | 3,3178 | 4,4485 | 0 |
| 1,5219 | 9,3985 | 3,0126 | 3,3091 | 0 |
| 1,9832 | 8,7639 | 3,8637 | 5,0358 | 21.1965 |
| 1,7145 | 7,964 | 3,9136 | 3,2594 | 0 |
| 1,7708 | 6,1871 | 3,8282 | 3,4199 | 0 |
| 1,5702 | 7,5744 | 3,9493 | 5,8405 | 46.6082 |
| 1,7553 | 6,6074 | 3,6952 | 5,0298 | 0 |
| 1,7355 | 6,4724 | 3,069 | 4,2154 | 0 |
| 1,8631 | 8,525 | 3,2842 | 4,9601 | 5.9804 |

| | | | | |
|---|---|---|---|---|
| 1,9466 | 8,982 | 4,0661 | 5,6656 | 41.4268 |
| 1,75 | 7,95 | 3,95 | 3,75 | 75.6561 |
| 1,8033 | 7,2032 | 3,4854 | 5,3227 | 59.8324 |
| 1,5281 | 6,8886 | 3,6034 | 4,3715 | 66.8742 |
| 1,6168 | 9,4247 | 4,0227 | 4,9908 | 60.1542 |
| 1,9524 | 7,1203 | 3,0068 | 4,9797 | 30.5815 |
| 1,7134 | 8,6318 | 4,0617 | 3,8533 | 79.7057 |
| 1,9136 | 6,8135 | 3,7111 | 3,5267 | 60.4265 |
| 1,8605 | 8,7347 | 4,0076 | 4,2923 | 75.6030 |
| 1,5486 | 8,9847 | 3,476 | 5,2441 | 53.6924 |
| 1,7526 | 9,3919 | 3,2343 | 5,2498 | 51.9170 |
| 1,8366 | 6,2819 | 3,9911 | 4,9275 | 56.2177 |
| 1,5445 | 8,4008 | 3,1652 | 5,7269 | 57.4061 |
| 1,788 | 6,6251 | 3,0249 | 3,6688 | 38.3356 |
| 1,6968 | 6,5889 | 3,8923 | 5,748 | 58.9163 |
| 1,947 | 9,347 | 3,2125 | 5,6498 | 47.6409 |
| 1,6344 | 7,2041 | 3,1312 | 4,7855 | 62.8422 |
| 1,7058 | 7,8329 | 3,3799 | 3,6989 | 68.3136 |
| 1,717 | 9,8053 | 3,0148 | 3,4475 | 39.9165 |
| 1,9312 | 6,6629 | 3,206 | 5,8107 | 45.7735 |
| 1,5226 | 6,6527 | 3,8245 | 5,529 | 57.7810 |
| 1,9046 | 9,2508 | 3,6227 | 4,027 | 37.5256 |
| 1,9428 | 9,5996 | 3,3578 | 3,0236 | 0 |
| 1,5737 | 7,9858 | 4,0514 | 4,5816 | 72.2466 |

**Table A1. 2.** 2nd O.F values for input variables; t, b, g, and h, circular rigid part

| t (mm) | g (mm) | h (mm) | b (mm) | 2nd O.F |
|---|---|---|---|---|
| 1.9466 | 4.0661 | 5.6656 | 8.9820 | 41.4300 |
| 1.7000 | 4.0500 | 3.8500 | 8.6500 | 0 |
| 1.5522 | 3.3414 | 5.4143 | 8.4431 | 40.9400 |
| 1.7232 | 3.3464 | 4.2313 | 9.6995 | 0 |
| 1.7542 | 3.3178 | 4.4485 | 7.0976 | 0 |
| 1.5219 | 3.0126 | 3.3091 | 9.3985 | 0 |
| 1.9832 | 3.8637 | 5.0358 | 8.7639 | 21.2000 |
| 1.7145 | 3.9136 | 3.2594 | 7.9640 | 0 |
| 1.7708 | 3.8282 | 3.4199 | 6.1871 | 0 |
| 1.5702 | 3.9493 | 5.8405 | 7.5744 | 46.6100 |
| 1.7553 | 3.6952 | 5.0298 | 6.6074 | 0 |
| 1.7355 | 3.0690 | 4.2154 | 6.4724 | 0 |
| 1.8631 | 3.2842 | 4.9601 | 8.5250 | 5.9800 |
| 1.3624 | 2.3368 | 9.9938 | 4.8340 | 0 |
| 1.5500 | 3.9500 | 7.5500 | 5.8500 | 46.4200 |
| 1.2961 | 2.9188 | 9.4066 | 5.2604 | 32.1100 |
| 1.6419 | 2.4042 | 8.1968 | 5.0495 | 0 |
| 1.4773 | 2.6939 | 6.9190 | 5.1933 | 21.9900 |
| 1.6422 | 3.9612 | 9.2798 | 4.1662 | 0 |
| 1.3696 | 3.8145 | 9.4232 | 4.8812 | 9.9200 |
| 1.7678 | 4.0111 | 8.0684 | 5.2307 | 35.8600 |
| 1.7396 | 2.9991 | 9.6230 | 4.3378 | 0 |
| 1.5486 | 4.0182 | 6.3987 | 4.3867 | 0 |
| 1.8712 | 2.3336 | 6.0531 | 4.0555 | 0 |
| 1.5410 | 2.3360 | 8.3830 | 5.2230 | 0 |
| 1.3263 | 2.8806 | 7.5943 | 4.2713 | 0 |
| 1.9479 | 3.6982 | 6.1743 | 4.8564 | 0 |
| 1.7500 | 4.0000 | 8.0500 | 5.2500 | 40.1200 |
| 1.3894 | 3.9664 | 7.3392 | 4.9206 | 0 |
| 1.7129 | 2.2596 | 7.7668 | 5.5658 | 0 |
| 1.7147 | 2.0981 | 9.5939 | 5.3739 | 0 |
| 1.4548 | 3.1776 | 7.4281 | 4.1403 | 0 |
| 1.8919 | 2.9743 | 6.0909 | 5.8241 | 27.3400 |
| 1.6384 | 3.2682 | 9.8448 | 5.6363 | 34.7100 |
| 1.4687 | 4.0360 | 7.7836 | 5.3958 | 39.6900 |
| 1.6041 | 3.4207 | 8.5139 | 4.2467 | 0 |
| 1.9229 | 2.5269 | 7.2481 | 5.8875 | 9.8700 |
| 1.3695 | 2.2481 | 6.4386 | 4.6053 | 0 |
| 1.4611 | 3.4764 | 9.0750 | 4.5651 | 0 |
| 1.9138 | 2.1004 | 9.7698 | 4.2489 | 0 |
| 1.5386 | 2.7425 | 6.7597 | 4.2926 | 0 |
| 1.4302 | 2.7395 | 7.9450 | 4.8171 | 0 |
| 1.8456 | 3.9193 | 6.0929 | 4.9005 | 0 |
| 1.5802 | 3.3196 | 9.7205 | 5.1931 | 35.4700 |
| 1.7500 | 4.0000 | 8.0000 | 5.2500 | 39.4000 |
| 1.5185 | 3.4798 | 7.8295 | 4.1864 | 0 |
| 1.9967 | 4.0608 | 7.0098 | 3.4864 | 0 |

| | | | | |
|---|---|---|---|---|
| 1.7181 | 3.0320 | 6.9323 | 4.8586 | 0 |
| 1.9768 | 3.1335 | 8.6283 | 4.0498 | 0 |
| 1.7619 | 3.0786 | 6.9648 | 3.1690 | 0 |
| 1.9165 | 3.7886 | 7.1278 | 5.6478 | 41.0200 |
| 1.8065 | 3.5697 | 9.7377 | 4.0272 | 0 |
| 1.7004 | 3.9913 | 7.2220 | 4.1576 | 0 |
| 1.8145 | 3.6749 | 8.0733 | 3.2535 | 0 |
| 1.7266 | 3.9535 | 7.6122 | 3.0939 | 0 |
| 1.6104 | 3.6099 | 9.8850 | 4.8094 | 0 |
| 1.9949 | 3.3543 | 7.3177 | 5.6446 | 37.6500 |
| 1.5006 | 3.8500 | 6.7542 | 5.0397 | 5.6900 |
| 1.7573 | 3.6468 | 8.5018 | 5.6192 | 43.1500 |
| 1.9500 | 3.6500 | 8.5000 | 5.6000 | 43.5800 |
| 1.7500 | 3.6500 | 8.5000 | 5.6000 | 43.1600 |
| 1.7500 | 3.8500 | 8.5000 | 5.6000 | 44.6200 |
| 1.7500 | 3.6500 | 8.7000 | 5.6000 | 43.5700 |
| 1.7500 | 3.6500 | 8.5000 | 5.8000 | 46.7100 |
| 1.5500 | 3.6500 | 8.5000 | 5.6000 | 37.4500 |
| 1.7500 | 3.4500 | 8.5000 | 5.6000 | 44.3500 |
| 1.7500 | 3.6500 | 8.3000 | 5.6000 | 42.1900 |
| 1.7500 | 3.6500 | 8.5000 | 5.4000 | 40.8600 |
| 1.8264 | 3.8000 | 8.5409 | 5.9000 | 45.8700 |
| 1.7684 | 3.5837 | 8.4984 | 5.8725 | 47.3300 |
| 1.7668 | 3.4876 | 8.4947 | 5.9000 | 45.7500 |
| 1.7775 | 3.6159 | 8.4871 | 5.9000 | 48.1100 |
| 1.7871 | 3.6643 | 8.4125 | 5.9000 | 46.2500 |
| 1.7793 | 3.6234 | 8.5312 | 5.9000 | 43.8300 |
| 1.7659 | 3.6109 | 8.4687 | 5.9000 | 47.9200 |
| 1.7825 | 3.6168 | 8.4875 | 5.8914 | 47.2300 |
| 1.7822 | 3.6219 | 8.4806 | 5.9000 | 46.8500 |
| 1.7767 | 3.6110 | 8.4875 | 5.8913 | 48.0800 |
| 1.7678 | 3.6159 | 8.4893 | 5.9000 | 47.7200 |
| 1.7800 | 3.6252 | 8.4898 | 5.9000 | 48.3000 |
| 1.7828 | 3.6325 | 8.4960 | 5.9000 | 49.2000 |
| 1.7850 | 3.6399 | 8.5024 | 5.9000 | 44.8400 |
| 1.7798 | 3.6342 | 8.4963 | 5.8906 | 48.5300 |
| 1.7867 | 3.6260 | 8.5025 | 5.9000 | 48.6900 |
| 1.8000 | 3.6500 | 8.5000 | 5.9000 | 46.0500 |

**Table A1. 3.** 2nd O.F values for input variables; t, g, and h, rectangular rigid part

| **t (mm)** | **g (mm)** | **h (mm)** | **2nd O.F** |
|---|---|---|---|
| 1.6000 | 3.5000 | 5.0000 | 0.7497 |
| 1.9000 | 3.5000 | 5.0000 | 0 |
| 1.6000 | 3.8000 | 5.0000 | 0.3775 |
| 1.6000 | 3.5000 | 4.7000 | 0 |
| 1.8000 | 3.7000 | 5.3000 | 0 |
| 1.6500 | 3.5500 | 4.8500 | 0 |
| 1.6000 | 3.6500 | 5.0000 | 0 |
| 1.7500 | 3.5000 | 5.0000 | 0 |
| 1.6000 | 3.5000 | 4.8500 | 0.3494 |
| 1.5000 | 3.7000 | 5.7000 | 3.1800 |
| 1.6511 | 3.1706 | 4.1532 | 0 |
| 1.7000 | 3.0000 | 5.7000 | 0 |
| 1.5804 | 3.4750 | 3.0874 | 0 |
| 1.6500 | 3.2000 | 4.5000 | 0 |
| 1.8874 | 3.5372 | 3.5639 | 0 |
| 1.5619 | 3.9312 | 3.9503 | 0 |
| 1.5000 | 3.4000 | 4.0000 | 0 |
| 1.7140 | 3.2906 | 3.8786 | 0 |
| 1.5859 | 3.2282 | 4.2461 | 0 |
| 1.5679 | 3.3150 | 5.0152 | 0.7225 |
| 1.5000 | 3.8000 | 4.4000 | 0 |
| 1.8246 | 3.0364 | 5.3317 | 0 |
| 1.5255 | 3.1489 | 4.0892 | 0 |
| 1.7619 | 3.9240 | 5.0309 | 0 |
| 1.7035 | 3.7813 | 5.5293 | 0.3504 |
| 1.6838 | 3.8489 | 3.5495 | 0 |

**Table A1. 4.** 3rd O.F values for input variables; t, s, g, d, and h, oval rigid part

| t (mm) | g (mm) | s (mm) | h (mm) | Θ (degree) | 3rd O.F |
|---|---|---|---|---|---|
| 2.0000 | 2.6000 | 0.60000 | 5.2500 | 52.000 | 54.423 |
| 2.0065 | 3.4270 | 0.84586 | 5.5745 | 39.955 | 44.316 |
| 1.9000 | 2.8000 | 0.40000 | 5.5000 | 49.000 | 30.363 |
| 1.4226 | 3.1455 | 0.87006 | 5.7969 | 37.325 | 39.495 |
| 1.9401 | 2.9162 | 0.50678 | 5.1759 | 52.804 | 48.069 |
| 1.6426 | 2.8846 | 0.56251 | 4.9146 | 55.072 | 43.895 |
| 1.8479 | 2.6127 | 0.60981 | 4.7527 | 55.590 | 45.661 |
| 1.7000 | 3.0000 | 0.80000 | 5.2000 | 40.000 | 42.754 |
| 1.8651 | 3.3062 | 0.64181 | 5.1355 | 43.451 | 45.424 |
| 1.6786 | 3.4863 | 0.94482 | 4.8659 | 40.518 | 19.340 |
| 2.2167 | 3.3911 | 0.49763 | 5.5344 | 50.464 | 41.091 |
| 1.7000 | 3.1000 | 0.50000 | 5.0000 | 36.000 | 45.907 |
| 2.0757 | 3.8648 | 0.26623 | 5.8808 | 56.118 | 10.280 |
| 1.7832 | 2.5454 | 0.65529 | 5.2351 | 47.949 | 54.505 |
| 1.4875 | 3.6296 | 0.29801 | 4.9744 | 59.322 | 14.211 |
| 2.4052 | 3.3047 | 0.91837 | 5.8419 | 34.129 | 44.444 |
| 2.0944 | 3.2850 | 0.84627 | 4.7272 | 39.627 | 25.757 |
| 1.5563 | 3.9615 | 0.57613 | 5.0520 | 49.834 | 33.096 |
| 1.8630 | 3.2751 | 0.49156 | 5.2951 | 44.686 | 40.401 |
| 1.7438 | 3.9028 | 0.75464 | 4.5911 | 39.745 | 0.31591 |
| 2.4784 | 3.1737 | 0.11585 | 4.5635 | 38.679 | 47.033 |
| 1.9449 | 3.7078 | 0.42952 | 5.7429 | 35.521 | 32.855 |
| 2.2684 | 3.6365 | 0.27856 | 4.8409 | 38.846 | 44.965 |
| 1.6366 | 3.7423 | 0.61868 | 5.8225 | 41.338 | 32.079 |
| 2.3172 | 3.3803 | 0.37134 | 5.5216 | 52.427 | 26.289 |
| 1.6526 | 3.0221 | 0.35580 | 4.7010 | 43.046 | 35.715 |
| 2.3188 | 3.4965 | 0.12425 | 4.5938 | 30.943 | 55.480 |
| 2.4775 | 3.7385 | 0.16567 | 5.7645 | 42.253 | 23.987 |
| 1.6947 | 3.9635 | 0.33325 | 5.7500 | 57.752 | 10.881 |
| 1.8067 | 3.8316 | 0.86451 | 5.4832 | 47.280 | 42.673 |
| 1.6423 | 2.9573 | 0.15120 | 4.6526 | 46.529 | 23.556 |
| 1.7975 | 2.8415 | 0.20509 | 4.9825 | 41.960 | 34.269 |
| 1.6792 | 3.1699 | 0.69710 | 5.7852 | 32.023 | 32.593 |
| 1.9436 | 2.8665 | 0.49209 | 5.1142 | 44.781 | 47.691 |
| 1.6836 | 2.9965 | 0.15043 | 5.0553 | 38.402 | 33.569 |
| 1.4618 | 3.2837 | 0.11684 | 5.2117 | 48.401 | 12.821 |
| 2.0038 | 3.3611 | 0.77749 | 5.4877 | 33.791 | 40.057 |
| 1.7183 | 2.8511 | 0.52095 | 5.8408 | 36.978 | 37.958 |
| 2.1916 | 2.7766 | 0.93718 | 4.5275 | 30.847 | 24.018 |

# Appendix 2

Figure A2.1 presents a MATLAB Surf Plot. The plot describes the effects of different limit values on the percentage of the nodal elements of the surface that satisfy the conditions based on these values. The limits are considered for the magnitude of the first principal strain and the allowable deviation in degree from the desired orientation of the first principal strain. Based on the behavior of the device, a choice in order of 10% for the magnitude of the strain and 5° for the angle is reasonable since 86% of the nodes satisfy these conditions. Higher magnitudes for the first principal strain and lower degree values for the angle decreases the percentage of nodal elements that satisfy the conditions to a low value of 20%.

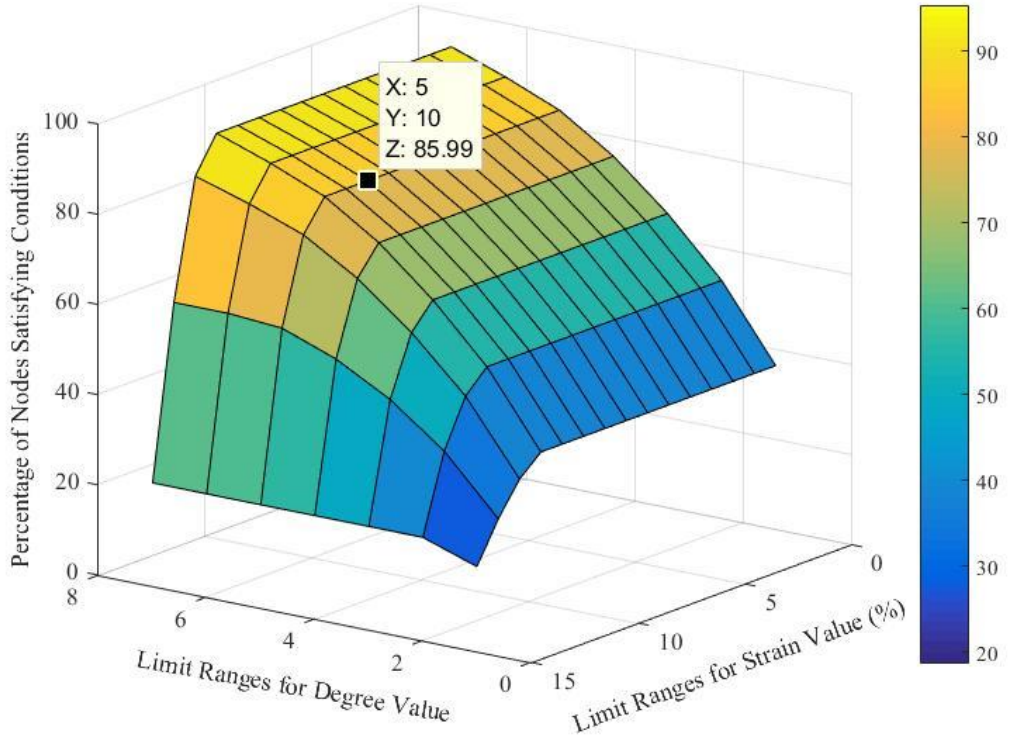


**Figure A2. 1.** Percentage of the nodes satisfying the conditions for different conditional limit values of the magnitude of the strain (%) and the allowable angular deviation from the determined orientation of the strain (degree)

# Appendix 3

This appendix presents an example definition of boundary conditions and mesh elements in the computational model. Figure A2.1 indicates regions that are considered to be fixed (left) and those that pressure load are applied (right). Figure A2.2 represents the tetrahedral mesh elements.

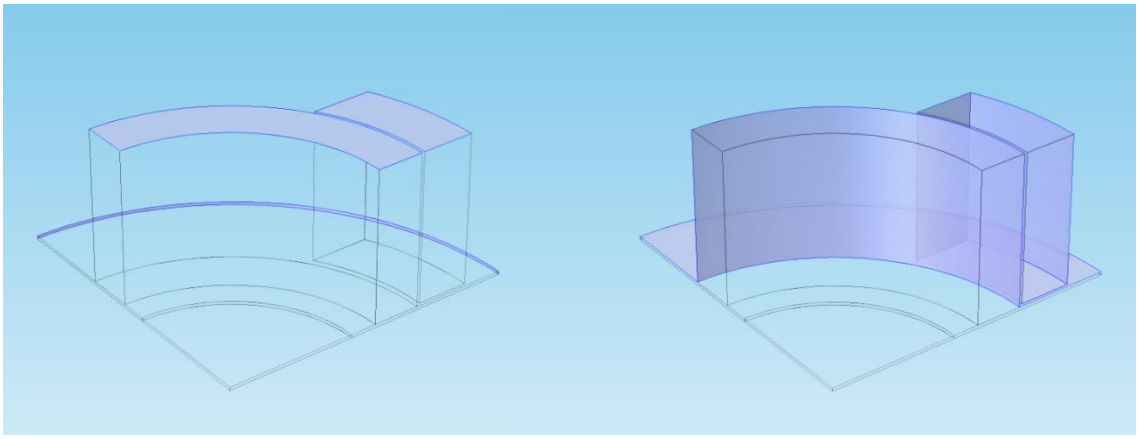

**Figure A3. 1.** Fixed constraint boundary condition regions (left) and load boundary condition regions (right)

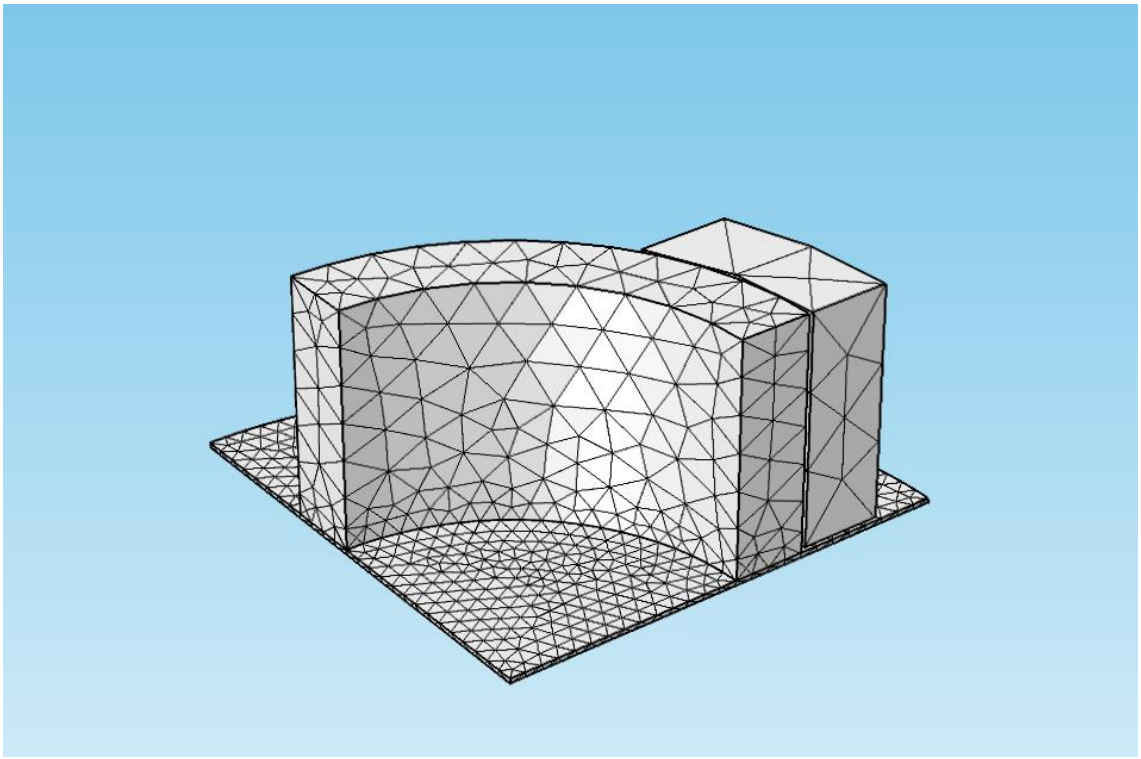

**Figure A3. 2.** Tetrahedral Mesh elements, complete mesh consist of 5951 domain elements, 3386 boundary elements, and 310 edge elements.